THE CONTACT AND COMPACTING PRESSURES INFLUENCES ON THE QUALITY OF THE FRICTION WELDED JOINT

Nada Ratković[1], Dušan Arsić[1], Vukić Lazić[1], Ružica Radoslava Nikolić[1,2,*], Branislav Hadzima[2]

[1]Faculty of Engineering, University of Kragujevac, Sestre Janjić 6, 34000 Kragujevac, Serbia
[2]Research Center, University of Žilina, Univerzitna 1, 010 26 Žilina, Slovak Republic

[*]corresponding author: e-mail: ruzicarnikolic@yahoo.com

Resume

The theoretical and experimental analyses of the friction welding pressure influence on the plastic deformation level and the quality of the friction welded joint are presented in this paper. The joint of the tempering and the High-Speed steel was realized by the friction welding. The objective was to relate the two basic process parameters - the friction and compacting pressures - to plastic deformation parameters during the friction welding of two the steels. The fact that materials are dissimilar additionally complicates the welding procedure and its analysis. The friction welding is a specific and complex process, since in the joint zone material is heated and plasticized with necessary action of the multi-step pressure to realize the joint. The total deformations in the axial and radial directions are directly dependent on the applied welding pressure. Considering that geometry and shape of the friction welded joint directly depend on the friction pressure, some welded joints' basic shapes obtained with various pressures are presented. The experimental investigation was conducted on cylindrical samples made of the two steels and the analysis of results served for establishing the influences of the friction and compacting pressures on changes of the steel samples dimensions and shapes.

Article info

Article history:
Received 11February 2016
Accepted 05 April 2016
Online 10 July 2016

Keywords:
Friction welding;
Friction pressure;
Compacting pressure;
High-Speed steel;
Tempered steel.

Available online: http://fstroj.uniza.sk/journal-mi/PDF/2016/07-2016.pdf

ISSN 1335-0803 (print version)
ISSN 1338-6174 (online version)

1. Introduction

The friction welding procedure was selected for joining of the two dissimilar steels. The experimental pair of materials consisted of two steels – the high speed steel (HSS) and the carbon steel for tempering. This selection is not arbitrary, but the decisive role had their application in industry, especially in the cutting tools manufacturing (such as drills, mills, etc.). The thermal and mechanical properties of those two steels are significantly different. This is why the friction pressure has the strong influence on the contact layers of those materials. The proper pressure selection ensures the balance between the quantity of the generated heat and plastic deformation in the phase of stable friction, since those steels possess different abilities for plastic deformation [1]. In addition, they also differ with respect to the strength level in the hot conditions, due to what an uneven line of joining would appear. The possibility of lack of penetration appears in the zones of sharp and deep jamming of the high speed steel into the tempering steel. This is why it is necessary to ensure the optimal thermal-deformation conditions, which will enable necessary plastic flow of material during the compacting and filling in the points where the penetration was missing. The mentioned conditions can be achieved properly by selecting the optimal values of the friction pressure and the compacting pressure. The friction welding process is being conducted due to the compressive stress action, set by the machine. That is the reason why in the friction welding of these two steels the risk of hot cracks appearance does not exist. It is the well-known fact that in welding by melting the HSS has strong proneness towards formation both of hot and cold cracks. That makes the justifiability of application of the friction welding even greater. The friction welding of the dissimilar steels was considered in papers [2 - 5]. In earlier research by authors of this paper it was shown that the joining of the two dissimilar steels can be realized, but that it is necessary to select the optimal welding parameters [1, 2]. Otherwise, the flaws in the joint may appear, like the lack of penetration or poor joint's geometry. In addition, in paper [3] are presented results, which are related to structural and chemical changes in the joint, as well as to the influence of the welding parameters on the joint deformation – shortening and joint diameter. Those results have shown that one of the most important parameters is the welding time and that by its extension the deformation of joints is increasing. The pressure increase causes increased shortening of the samples, where the tempering steel one is more shorten than the HSS sample. Similar investigations were conducted by Savić et al. [4], who were measuring the temperature cycles and monitoring the micro structure of the joint's zones in welding of the high speed steel HS 6-5-2C and the carbon steel C60 and made an attempt to make a model of the friction welding. In further research, Handa and Chawla [5] have presented a study of continuous drive friction welding of austenitic stainless steel and ferritic steel combinations. The major contribution of their study consisted of the friction welding process parameters optimization, mechanical characterization, micro structure and fracture behavior analyses. Their experimental results indicated that the axial pressure has a significant effect on the mechanical properties of the joint and that it is possible to increase the quality of the welded joint by selecting the optimal axial pressure. The same authors in paper [6] have determined the strength of the joint by means of mechanical properties such as torsional strength, impact strength and micro hardness. The experimental results indicate that the rotational speed and the axial pressure have a significant effect on mechanical properties of the joint and that it is possible to improve the quality of the joint by selecting the optimal parameters.

Studies of numerous advantages of the friction welding procedure with respect to other welding processes and obtaining of the high quality joints of excellent physical, mechanical, technological and other properties were conducted in papers [7 - 10]. Veljić et al. [7] have shown that the friction welding procedure has advantages related to health and environmental protection and work safety. This refers, primarily, to lowering the emission of gasses and harmful radiation, which are present in the arc welding procedures. The quality of the friction stir welding joints was analyzed in works by Dascau et al. [8] and Eramah et al. [9], where the joints' impact toughness was tested on the Charpy pendulum with separated energies of the crack initiation and separation. It was shown that the highest influence on the crack initiation energy exhibit the rotation velocity (42 %) and the tool angle (39 %), while the rotation velocity imposes the strongest influence on the crack propagation energy (63 %). All these also point to necessity of selecting the optimal welding parameters. Influences of the immersion phase and the tool penetration angle were studied by Veljić et al. in [10], where it was shown that the increase of the tool rotation causes decrease of the maximal temperature zones, what can later lead to improvement of the joint's mechanical properties. Mechanical tests of the aluminum-copper joint were the subject of research in [11], where it was shown that the tensile strength of the joint depends to the largest extent on the welding time and that it has to be longer than 10 s in order to obtain the maximal tensile strength. In addition, besides the mechanical properties, some very important research on the wear resistance of the friction welded joints was done in paper by Kumar et al. [13].

2. General remarks on friction welding

The friction welding (FW) belongs into a group of welding procedures under pressure, i.e. it is the type of welding where the deformation cycle is dominant. The friction welding is, by its nature, the compound of thermal and mechanical phenomena, mutually conditioned and dependent on the base materials' properties. The joint is being realized due to action of the heat released due to friction on the contact surfaces between the base materials. The heat generation is strictly localized and it occurs in the narrow layers in the friction zone. The joint is created at the temperature, which is lower than the base materials' melting temperatures, when the materials are in the plasticized state and when, due to action of the compressive force, the welding occurs.

In continuous friction welding one welded element is rotating with certain speed, while the other element is moving translatory along the straight line towards the first one, Fig. 1. The initial phase of friction begins when the first contact is established between the welded elements. During that confronting of the cylindrical elements the very complex changes of materials are happening in the contact zone within the short time interval.

The process of friction welding actually consists of the two phases: the first is the friction phase, which is characterized initially by the mutual interactions of the very small particles of the two materials, which is then followed by the intensive wear all the way up to transition into the stable friction. The mixing of the highly plasticized particles occurs in the contact zone. The friction pressure corresponds to this phase, Fig. 1. The second phase consists of compacting, when the pressure is increasing until the compacting pressure p_c is reached. The rotation of the welded element is then stopped by abrupt braking. The maximum plastic deformation is then reached. The contact layers of the welded parts are coming to a distance as close as the crystal lattice parameters and the joining occurs.

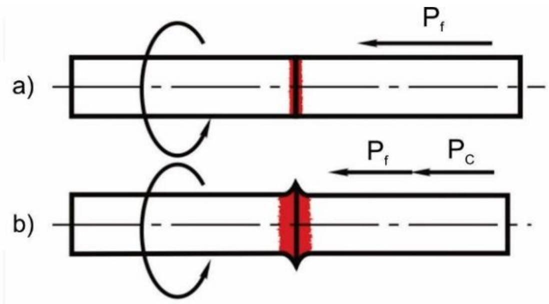

Fig. 1. Schematics of the friction welding:
(a) the friction phase; (b) the compacting phase.
(full colour version available online)

The specific phenomenon during the FW of these two dissimilar steels is hard facing of the high speed steel onto the tempering steel's surface, even during the friction phase. The hard faced layer of the HS steel is about 10 to 200 μm thick, thus the friction pair actually becomes the HS steel-HS steel joining.

3. The friction pressure and the compacting pressure

The pressure in the friction phase has a significant influence on the thermal-deformation phenomena. The pressure action causes intensive deformation of the materials' surface layers, heat release and increase of temperature. In the final phase of the FW cycle, the pressure ensures closing of the contact surfaces to each other at the submicroscopic distances. It also ensures the extrusion of the surplus material and the remaining impurities from the joining spot at the flange, where the so-called "mushroom" is formed. The two-step pressure variation was applied during the experimental part of this research, Fig. 2.

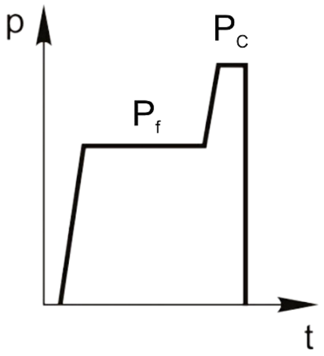

Fig. 2. The pressure variation with time: p_f – the friction pressure, p_c – the compacting pressure.

Besides the various forms of the two-step cycles, some recommendations exist for the three-step pressure variations. It was shown that in the friction welding of the two similar materials of the same cross-section, the same efficiency is achieved by application of the continuous or any other type of the step-wise pressure cycle, while for welding of the dissimilar materials it is necessary to apply the multi-step pressure variation cycle.

The proper selection of the friction pressure (p_f) ensures the balance between the quantity of the released heat and the plastic deformation, in the stable friction phase, [6]. If the applied pressure is too small, the necessary heating of the frontal surfaces cannot be realized, since the quantity of the released heat is small with respect to heat, which is being taken by conduction into the base material, namely into the extruded material of the wreath. In addition, the undesired phases would not be squeezed out from the joining zone, what would create the unfavorable conditions for the final compacting. At the lower pressures, than the optimal values, the axial deformation is reduced. That is manifested by appearance of the zones where the elementary joints were created only spot-wise. Such zones have the shape of the broken concentrically positioned ring-like surfaces where the lack of penetration occurs. It is recommended that the friction welding should be executed with pressures which are proportional to the strength of the base materials at the forging temperature [1]. If the pressure level is higher than the optimal value, the completely different configuration of the joint would appear and the unwanted larger quantity of the material would be extruded into the joint's wreath, Fig. 3.

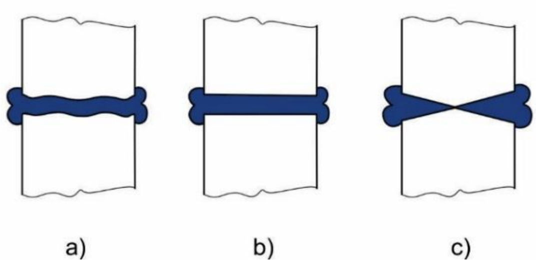

Fig. 3. Influence of the friction pressure pf on the joint shape: (a) too small value, (b) optimal value; (c) too large value.
(full colour version available online)

4. Experimental investigation

The experimental part of this research consisted of the friction welding of elements made of the high speed steel HS 6-5-2-5 and steel for tempering C60, Fig. 4a, executed on the friction welding machine with continuous drive, Fig. 4b. The objective of the experiment was to establish the influence of the friction and compacting pressures on the plastic deformation parameters and the quality of the welded joint.

The recommended values of the friction pressure are 10 to 110 MPa and of the compacting pressure 20 to 320 MPa. In the conducted tests the friction pressure values were p_f = 70, 80 and 90 MPa, while the ratio of the compacting and the friction pressures was p_c/p_f = (2.2 – 2.8). Measurements were done for different welding times.

5. Results and discussion

Monitoring of the axial force was done by measuring the change of length of both welded steels' elements. Results are presented by graphs in Fig. 5, for three values of the friction pressure of 70, 80 and 90 MPa.

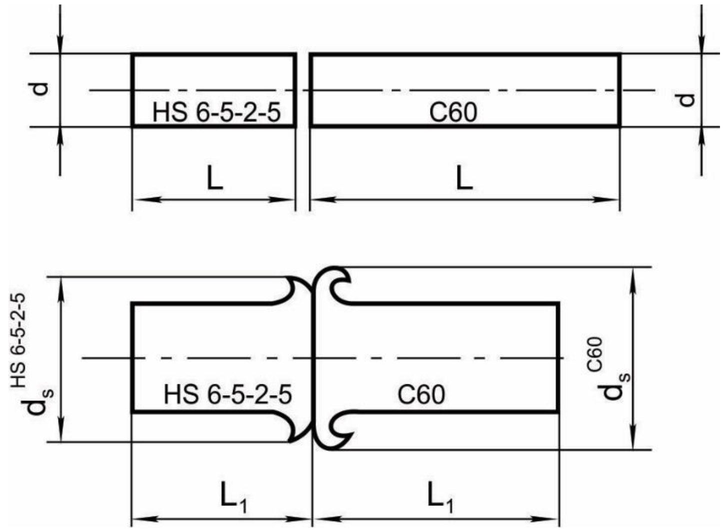

a) elements of the steel pair (HS 6-5-2-5/C60): prior to welding (above) and after the welding (below)

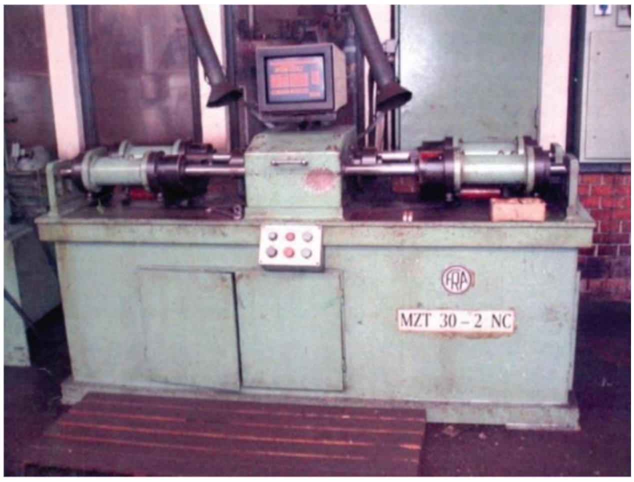

b) the friction welding machine MZT 30-2 NC
Fig. 4. Friction welding of elements.
(full colour version available online)

According to results, presented in Fig. 5, one can notice that shortening of the element made of the C60 steel for tempering was significantly bigger than shortening of the element made of the high speed steel HS 6-5-2-5. It can also be observed that during the first 10 s of friction, when the pressure is increasing, the shortening increase per time unit is somewhat smaller. For instance, the element of the tempering steel C60 shortened for 6.8% for 10 s, while in the next 8 s the shortening reached 10.8%; the element made of the steel HS 6-5-2-5 was shortened for 5.2 % during the first 10 s and then in 8 s for 7.4%. This is the consequence of the narrow zone, which is heated up to the elevated temperatures, namely the narrow heat affected zone, for both materials. At the constant friction pressure, the extrusion of the heated metal out of the joining zone is smaller, since the deformation resistance is higher.

Variation of the samples' wreath diameters in the joint zone, for both materials, expressed in % is shown in Fig. 6. Results given in this figure are obtained for the friction pressure of 90 MPa and the compacting pressure of 200 MPa. Analyses have shown that the variation of the extruded materials diameter depends more on the duration of friction than on the friction pressure.

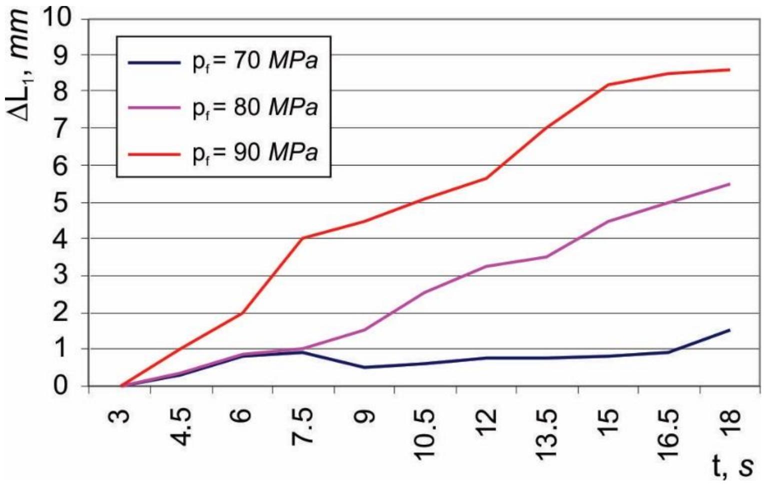

a) C60 sample

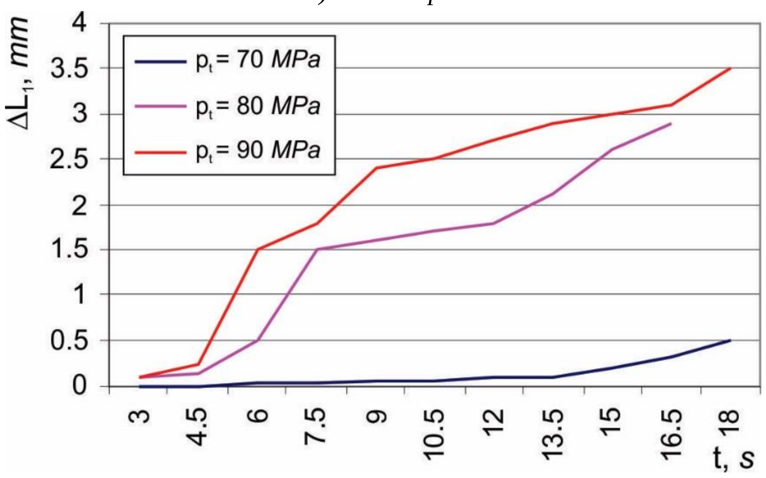

b) HS 6-5-2-5 sample

Fig. 5. Graphical presentation of the samples shortening in terms of time.
(full colour version available online)

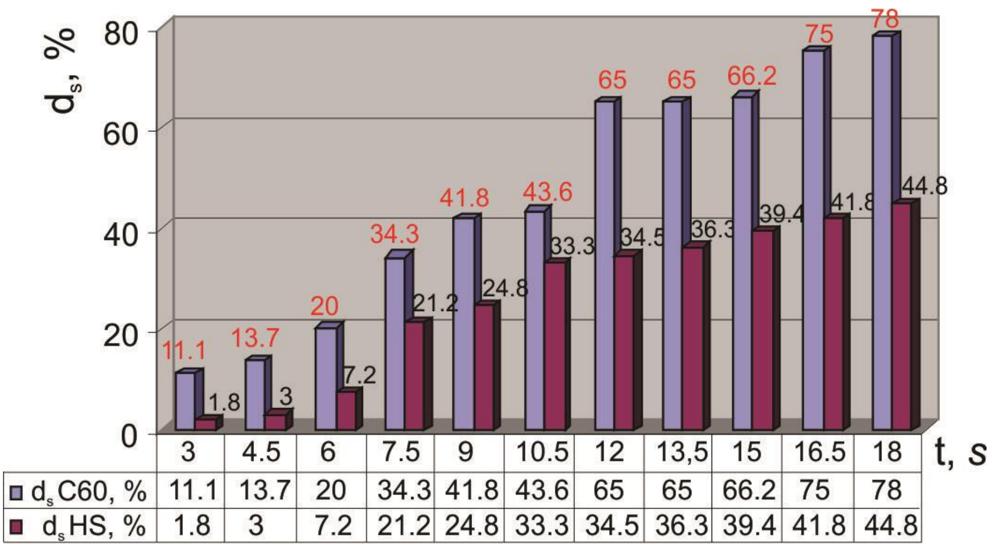

t, s	3	4.5	6	7.5	9	10.5	12	13,5	15	16.5	18
d_s C60, %	11.1	13.7	20	34.3	41.8	43.6	65	65	66.2	75	78
d_s HS, %	1.8	3	7.2	21.2	24.8	33.3	34.5	36.3	39.4	41.8	44.8

Fig. 6. Variation of the wreath diameter (ds) at the joint spot in terms of the friction time, for both elements at pf = 90 MPa and pc = 280 MPa.
(full colour version available online)

6. Conclusion

The quality of the joint, realized by the friction welding, cannot be defined based on a single parameter, only. However, it could be established how each particular parameter, within range of its values, contributes to that quality. Due to the complexity of the friction welding process, one should investigate all the relevant parameters, like the friction and the welding times, which, in the proper correlation with the pressure, enable obtaining of the best results. One should also study influence of the welding speed, i.e. the number of rpms, then temperature and other parameters, as well as the metallurgical indicators. All these are even more prominent when the friction welding is used for joining the two dissimilar materials.

Considering the pressure, as one of the most important process parameters in the friction welding, it was shown in this paper that its influence on unfolding and results of the plastic deformation, and by that on the quality of the realized joint, is very important. By measuring and analysis of the investigated parameters, related to plastic deformation (samples' shortening, wreath diameter changes), one can come up with the feedback information, which helps in determining the interval of the optimal values of the considered process parameters (friction and compacting pressures in this case).

Acknowledgement

This research was partially financially supported by European regional development fund and Slovak state budget by the project "Research Centre of the University of Žilina" - ITMS 26220220183 and by the Ministry of Education, Science and Technological Development of Republic of Serbia through grants: ON174004, TR32036, TR35024 and TR33015.

Note

The shorter version of this research was presented at the SEMDOK 2016 International Seminar, 27. – 29. January, 2016, Terchová, Slovak Republic, reference [14].

References

[1] N. Ratković: Modeling of the machine parts of various forms of the welding process, Doctoral dissertation, Faculty of Mechanical Engineering, Kragujevac, Serbia, 2009.

[2] N. Ratković, A. Sedmak, M. Jovanović, V. Lazić, R. Nikolić, B. Krstić: Tehnički vjesnik - Technical Gazette 16(3) (2009) 27-31.

[3] N. Ratković, R. Nikolić, I. Samardžić: Metalurgija - Metallurgy 53(4) (2014) 513-516.

[4] B. Savić, S. Marković, R. Ćirić: FME Transactions 36(2) (2008) 93-97.

[5] A. Handa, V. Chawla: Mater. Eng. - Mater. Inž. 20(3) (2013) 102-111.

[6] A. Handa, V. Chawla: Mater. Eng. - Mater. Inž. 21(3) (2014) 94-103.

[7] D. Veljić, A. Sedmak, M. Rakin, N. Radović, N. Popović, H. Dascau, N. Bajić: Structural Integrity and Life 15(2) (2015) 111-116.

[8] H. Dascau, S. Kirin, A. Sedmak, A. Eramah, S. Tadić: Structural Integrity and Life 15(1) (2015) 51-54.

[9] M. M. A. Eramah, S. Tadić, A. Sedmak: Structural Integrity and Life 13(3) (2013) 171-177.

[10] D. Veljić, M. Perović, A. Sedmak, M. Rakin, N. Bajić, B. Medjo, H., Dascau: Structural Integrity and Life 11(2) (2011) 131-134.

[11] N. Ratković, A. Sedmak, M. Jovanović, V. Lazić, R. Nikolić, B. Krstić: Tehnički vjesnik - Technical Gazette 16(3) (2009) 3-7.

[12] N. Ratković, D. Arsić, V. Lazić, R. Nikolić, B. Hadzima: Procedia Engineering, (2016) (in press).

[13] R. Kumar, S. Chattopadhyaya, S. Hloch, G. Krolczyk, S. Legutko: Eksploatacja I Niezawodnosc – Maintenance and Reliability 18(1) (2016) 128-135.

[14] N. Ratković, D. Arsić, V. Lazić, R. Nikolić, B. Hadzima: In Proc. of Abstracts of "SEMDOK 2016" - 21st International Seminar, Terchova, Slovakia 2016, p. 9.

EFFECT OF TOOL SHAPE AND WELDING PARAMETERS ON MECHANICAL PROPERTIES AND MICROSTRUCTURE OF DISSIMILAR FRICTION STIR WELDED ALUMINUM ALLOYS

Chetan Aneja[1,*], Amit Handa[1]

[1] RIMT-Institute of Engineering & Technology, Mandi Gobindgarh (Punjab), India

[*]corresponding author: e-mail: chetananeja26@gmail.com

Resume

In the present experimental study, dissimilar aluminum alloy AA5083 and AA6082 were friction stir welded by varying tool shape, welding speed and rotary speed of the tool in order to investigate the effect of varying tool shape and welding parameters on the mechanical properties as well as microstructure. The friction stir welding (FSW) process parameters have great influence on heat input per unit length of weld. The outcomes of experimental study prove that mechanical properties increases with decreasing welding speed. Furthermore mechanical properties were also found to improve as the rotary speed increases and the same phenomenon was found to happen while using straight cylindrical threaded pin profile tool. The microstructure of the dissimilar joints revealed that at low welding speeds, the improved material mixing was observed. The similar phenomenon was found to happen at higher rotational speeds using straight cylindrical threaded tool.

Article info

Article history:
Received 24 January 2016
Accepted 31 May 2016
Online 10 July 2016

Keywords:
Friction Stir Welding;
AA5083 & AA6082 Al Alloys;
Tool Rotational Speed;
Welding Speed & Tool Shape;
Mechanical Properties & Microstructure.

Available online: http://fstroj.uniza.sk/journal-mi/PDF/2016/08-2016.pdf

ISSN 1335-0803 (print version)
ISSN 1338-6174 (online version)

1. Introduction

Joining of dissimilar metals is one of the most essential needs of industries [1]. In fact, dissimilar joining could be regularly faced in many series of developments including automotive, aerospace, electronics and shipbuilding industries, where fusion welding simply is not appropriate due to the large difference of physical and chemical properties between the components to be joined. Unfortunately, dissimilar metal welding has several fabrication and metallurgical drawbacks that can often lead to in-service failure [2]. Problems including porosity formation, solidification cracking and chemical reaction may occur during fusion welding of dissimilar materials although sound welds may be obtained in some limited cases with special attentions to the joint design and preparation, process parameters and filler metals.

Friction stir welding (FSW), a solid state joining technology, was invented in 1991 by The Welding Institute (TWI) of UK [3]. It is an eco-friendly fabrication technique, involving energy efficiency and versatility to provide satisfactory combination of microstructure and mechanical properties of assemblies [4]. For joining light metals, especially aluminum and its alloys, this technique avoids the formation of solidification cracking and porosity [5]. FSW also reduces the presence of distortions and residual stresses [6]. Moreover it significantly improves weld properties.

FSW is an appropriate solid state welding technique to effectively join any combination of dissimilar aluminum alloys [7]. In friction stir welding, a non consumable tool with a profiled pin is rotated and slowly plunged into the joint line between the two pieces of plate material, which are butted together. Frictional heat is generated between the wear resistant welding tool and the material of the work-pieces. This heat causes the latter to soften without reaching the melting point and allows traversing of the tool along the weld line. The plasticized material is transferred from the leading edge of the tool to the trailing edge of the tool pin and is forged by the intimate contact of the tool shoulder and the pin profile. It leaves a solid phase bond between the two pieces [8]. The advancing side (AS) is the side where the velocity vectors of tool rotation and traverse direction are similar and the side where the velocity vectors are opposite is referred as retreating side [9]. FSW parameters are tool geometry, axial force, rotational speed and traverse speed [10]. Characteristics of friction stir welded joints are influenced by material flow and temperature distribution across the weld which are dictated by tool design and welding parameters such as welding speed and tool rotational speed. Tool design is one of the most important factors to consider when designing a FSW joining process. The tool must perform many functions, including generating heat, promoting mixing, breaking up the joint line, dispersing oxide layers, creating forging pressure, containing material within the joint, thereby preventing surface weld flash, and preventing the formation (or minimizing the impact) of defects such as wormholes, sheet-thinning, or hooking defects [11]. The rotation of tool results in stirring and mixing of material around the rotating pin and the translation of tool moves the stirred material from the front to the back of the pin and finishes welding process.

Some studies on friction stir welding of aluminum alloy joints were reported in the literatures. Aval et al. [12] reported that at low tool rotational speed, insufficient material transportation as well as low heat generation by plastic deformation and friction at tool/workpiece interface may be responsible for producing poor quality of welds. Yuqing et al. [13] observed that tool pin profile could significantly influence material flow and peak temperature of the nugget zone which further effect microstructure evolution and mechanical properties of the weld. Dinaharan et al. [8] reported that tool rotational speed was a significant FSW parameter. Khodir and Shibayanagi [14] revealed that the grain size decreases with increasing welding speed. Grain size decreases due to the lower temperature caused by the lower heat input associated with faster welding speed. Sharma et al. [15] evaluated that at low welding speed, weld nugget was more homogeneous because high heat input per unit weld length resulted in more homogeneous temperature distribution and effective recrystallization. Palanivel et al. [7] studied that friction stir welding at higher welding speeds resulted in a shorter exposure time in the weld area with insufficient heat and poor plastic flow of the metal and caused some voids like defects in the joint. Ilangovan et al. [16] investigated that each pin profile had its own material flow characteristics like higher mixing of materials, reduction of TMAZ, HAZ regions. The joining of the materials of the weld interface is achieved by the frictional heat generated between the tool and the work-piece and the material flow.

The present work is aimed to the evaluation of the welding speed and tool rotational speed effect by varying tool shape on mechanical properties and microstructural behaviour of aluminum alloy AA5083 and AA6082 welded plates with thickness 6 mm, obtained by friction stir welding.

2. Experimental Methodology

The Friction stir welding set up was fabricated on CNC Vertical Milling Machine installed at Central Tool Room, Ludhiana. A clamping Fixture was utilized in order to fix the specimens to be welded on a milling machine. The tool was mounted on the vertical spindle. Friction stir weld was made of 5083 and 6082 aluminum alloy plates using welding speed of 20, 40 and 60 mm·min^{-1} and tool rotary speed of 1000 and 1200 rpm. AA5083 aluminum alloy was placed in the advancing side and AA6082 aluminum alloy was placed in the retreating side. The dimensions of aluminum alloy plates were 75 mm in width, 120 mm in length and 6 mm in thickness. The two prepared aluminum pieces were firmly clamped into the fixture. The rotating tool was made to pass through from the butt joint. Afterwards within a fraction of time, the sufficient heating was achieved due to the rubbing action between tool and plates. The bed was given automatic feed, along the joint direction. In this way welding was achieved. Friction stir welding process of two aluminum plates is shown in Fig. 1.

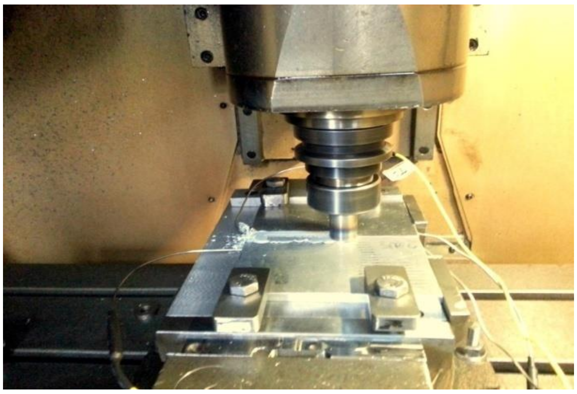

Fig. 1. Friction stir welding process.
(full colour version available online)

The two tools were prepared from EN8 Carbon steel material. One tool has straight cylindrical threaded pin and second tool has square pin as it was desirable that the tool must be hard to wear, tough and strong. Two types of EN8 carbon steel tools are shown in Fig. 2. The shoulder diameter and the shoulder height of the tool for FSW were 18 mm and 65 mm. The probe had a diameter of 6 mm and a height of 5.7 mm.

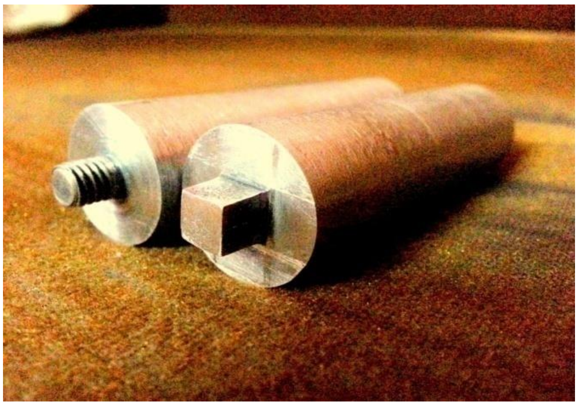

Fig. 2. EN8 carbon steel tool.
(full colour version available online)

5083 Aluminum-magnesium alloys are strain hardenable and have excellent corrosion resistance, toughness, weldability and moderate strength. 6082 aluminum-magnesium-silicon alloys are heat treatable and have high corrosion resistance, excellent extrudibility and moderate strength (Gungor et al., 2014). Especially with their high corrosion resistance and moderate strength, these alloys are widely used in shipbuilding industry. In this experimental work, the plates were prepared with 150×120×6 mm^3 dimensions. The chemical composition of AA5083 and AA6082 aluminum alloys presented in Table 1 and Table 2.

Table 1

Chemical composition of 5083 aluminum alloy (wt %).

Cu	Si	Zn	Mn	Mg	Fe	Ti	Cr	Al
0.03	0.1	.03	0.66	4.5	0.16	0.07	0.06	Balance

Table 2

Chemical composition of 6082 aluminum alloy (wt %).

Cu	Si	Zn	Mn	Mg	Fe	Ti	Cr	Al
0.05	1.0	0.05	0.70	0.8	0.16	0.05	0.06	Balance

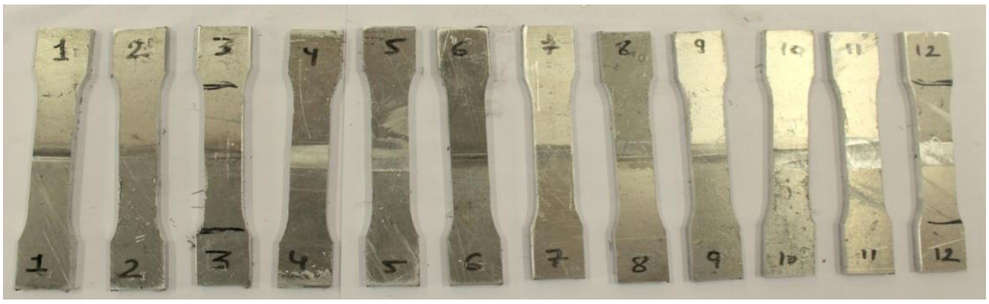

a) tensile test specimens

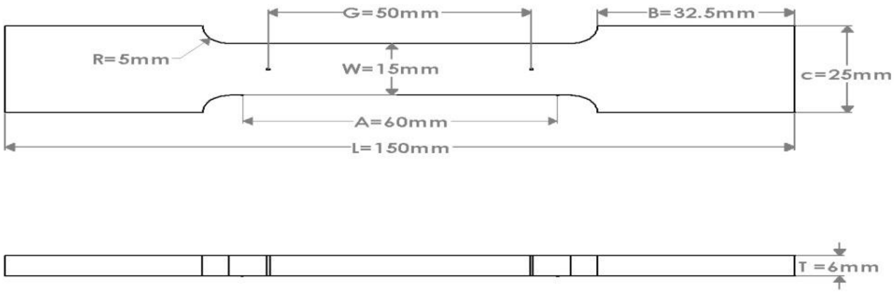

b) dimensions of Tensile test specimen

Fig. 3. Tensile test specimens

(full colour version available online)

2.1 Mechanical Testing and Microstructural Analysis

Friction stir welded parts were subjected to variety of mechanical tests to determine their suitability for the anticipated service applications. They were necessary to carry out so as to ensure the quality, reliability and strength of the welded joints.

2.1.1 Tensile Test

Tensile test was performed on universal testing machine, Model UT100, capacity of 1000KN, least count is 0.05 KN at CITCO Chandigarh. Tensile test specimens and dimensions of tensile specimen are present in Fig. 3(a) and 3(b). The standards were taken from ASTM (American society for testing and material) Internationals. Dumbles for tensile test were cut on FN2U Horizontal Milling Machine. The rotational speed used for dumble cutting was 450 rpm and Milling Cutter was used.

2.1.2 Micro Hardness

A Vickers micro hardness tester (Make FIE, Model No HV 50, CITCO Chandigarh) was employed for measuring the hardness across the transverse section of the joint with a load of 9.8 N and dwell time of 15 sec.

2.1.3 Microstructure

Metallographic specimens were cut mechanically from the welds and polished using abrasive disks and cloths. The chemical etchant to reveal the microstructure of the weld region was the Keller’s reagent (1 ml hydrofluoric acid, 1.5 ml hydrochloric acid, 2.5 ml nitric acid and 95 ml water). The microstructures were observed on optical microscope.

3. Results and Discussion

The Friction Stir welding has been done by varying tool pin profile, tool rotational speed and welding speed. The different combinations of tool pin profile, tool rotational speed and welding speed were taken. In this way 12 different friction stir weld joints were fabricated in this research work. The welding parameters were selected as per the Table 3. After the experiments, the pieces were cut into the samples of required dimensions for performing the tensile tests, microstructure observation and micro hardness testing.

3.1 Tensile Test Results

The ultimate tensile strength of FSW joints by varying tool pin profile, welding speed and tool rotational speed is shown in Fig. 4 (a-b). The results show that the tensile strength of the welded joints was improved by decreasing welding speed and by increasing tool rotational speed when the straight cylindrical threaded pin profile tool was used. The highest tensile strength of 121 MPa was reached for the joint produced by straight cylindrical threaded tool at welding speeds of 20 mm·min^{-1} and tool rotational speeds of 1200 rpm. This might be due to the reason that the welding speed influences the heat input per unit length of weld which further controls the degree of softening as well as the flowability of the plasticized material. At lower welding speeds, the quantity of heat supplied to the plasticized deforming material in the weld zone is greater and therefore wider is the softened area around the stirring tool leading to more improved metal flow and hence more effective bonding in the weld. This improved of the material flow and effective bonding leads to more homogeneity of the weld zone which resulted in higher tensile strength as the welded joints having higher heat input per unit length. A lower tensile strength of 102 MPa was observed in the joints made by square tool at welding speeds of 60 mm·min^{-1} and tool rotational speeds of 1000 rpm. At higher welding speeds, tool results in lower heat input per unit length of weld which in turn reduces stirring action of the material due to poor flowability in the weld area resulting in poor tensile strength, which decreases significantly when welding speed is increased and attributed the same to the formation of voids due to poor consolidation of weld interface at higher welding speed hence low heat input per unit weld length. Similar results were obtained by Sharma et al. [15]. Table 3 presents, the effect of tool pin profile, tool rotational speed and welding speed on the ultimate tensile strength.

Table 3

Ultimate Tensile Strength Results.

S No.	Tool Rotational Speed (rpm)	Welding Speed (mm·min^{-1})	Tool Pin Shape	Ultimate Tensile Strength (MPa)	S No.	Tool Rotational Speed (rpm)	Welding Speed (mm·min^{-1})	Tool Pin Shape	Ultimate Tensile Strength (MPa)
S-1	1000	20	Straight Cylindrical Threaded	119	S-7	1200	20	Straight Cylindrical Threaded	121
S-2	1000	40	Straight Cylindrical Threaded	113	S-8	1200	40	Straight Cylindrical Threaded	117
S-3	1000	60	Straight Cylindrical Threaded	103	S-9	1200	60	Straight Cylindrical Threaded	108
S-4	1000	20	Square Pin	110	S-10	1200	20	Square Pin	112
S-5	1000	40	Square Pin	110	S-11	1200	40	Square Pin	110
S-6	1000	60	Square Pin	102	S-12	1200	60	Square Pin	107

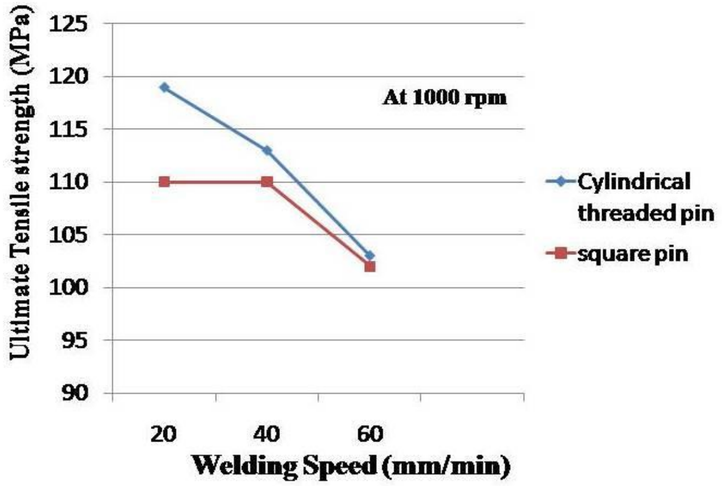

a) at 1000 rpm

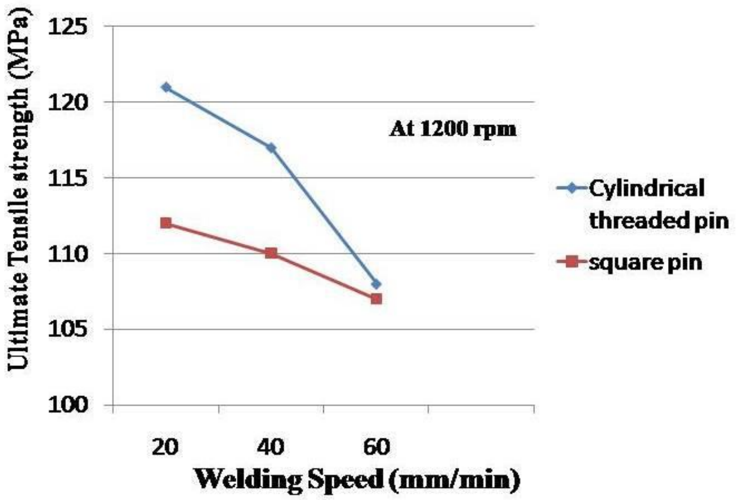

b) at 1200 rpm

Fig. 4. Ultimate tensile strength.

(full colour version available online)

Furthermore it has been noticed that as the rotational speed increases, the heat input within the stirred zone also increased. This might be attributed that at higher frictional conditions, more heat has been generated which resulted in more intense stirring and mixing of materials. As the spindle speed increased from 1000 rpm to 1200 rpm, the strength of the welded joints improved resulting higher heat generation which resulted in turn improved bonding. This behavior might be attributed to increase in solute concentration and number of new grains in the weld nugget due to higher heat input which led to improved tensile properties. Tang et al. [17] reported that peak temperature increased by 40°C within the weld zone with increase in rotary speed from 300 rpm to 650 rpm at constant welding speed of 120 mm·min^{-1}.

The dissimilar joints fabricated using the straight cylindrical threaded tool have higher values of the tensile strength when compared to the joints fabricated using square tool. The straight cylindrical threaded type of tool pin profile allow good material stirring quality and mixing of dissimilar plasticized metals during welding. The severe plastic deformation due to intense stir of cylindrical threaded pin profile results in higher strain energy relative to square pin profile. Square type of tool pin profile allow insufficient mixing of dissimilar plasticized metals because tool pin is incapable of deforming appropriate amount of metal during rotation which leads to low tensile strength. Same trends have been noticed by Ilangovan et al. [16] for ultimate tensile strength of friction stir welded joints of aluminum alloys.

3.2 Micro Hardness Test Results

Micro hardness test was performed in order to characterize the hardness in the vicinity of the weld affected area. The micro hardness tests were performed on a cross section perpendicular to the weld line, at mid thickness across the weld zone and into the base material, using 9.8 N load for a dwell period of 15 sec. The micro hardness variation across the weld nugget is shown in Fig. 5. The Vickers micro hardness varied from 90 HV to 95 HV in the base metal of AA5083 and varied from 98 to 105 HV in the base metal of AA6082. In the weld nugget zone hardness varied between 63 to 83 HV. The micro hardness measured from these welds showed that the microhardness was higher on the AA5083 side and lower on the AA6082 side. The thermo mechanically affected zone (TMAZ) on the AA6082 side had the lowest hardness and was found to varied from 51 to 68 HV. The graph indicates the decreasing trend of hardness from AA6082 HAZ to TMAZ region.

The average microhardness in the weld nugget decreased with increase in welding speed from 20 to 60 mm·min^{-1} and completely reverse trend was notice with the increase in tool rotation speed from 1000 to 1200 rpm. In the AA6082 side rapid decrease in hardness can be observed which may be attributed to the imposed thermal cycles as well as severe hot deformation. This leads to elimination of the precipitation hardening effect in the alloy owing to partial or complete dissolution of the hardening particles. Because of dissolution of the hardening phases in the TMAZ softening has been observed. On the stir zone, the increase in microhardness was associated with re-precipitation of fine particles. In the AA5083 side, because of recrystallization and generation of fine grains in the weld nugget the microhardness was found to be higher. As the tool rotational speed increased and welding speed decreased, more efficient mixing of the material were happened. The decrease in welding speed and increase in tool rotational speed would increase the heat input per unit weld length. The improved weld nugget hardness was due to the reduction in the density of coarse second phase strengthening particles. Similar results have been revealed by Aval et al. [12] for microhardness of friction stir welded joints. Gungor et al. [18] also made similar observations.

The hardness variation of each region of both tool pin profile was plotted and presented in Fig 5. The graphs indicate the decreasing trend of hardness from NZ to TMAZ in AA6082. The TMAZ zone of AA6082 was identified as the soften region in microhardness plot for both the pin profile. In the AA5083 side, no such variation in hardness was observed. The straight cylindrical threaded pin profile showed higher hardness than that of with square pin profile in the stir zone. The straight cylindrical threaded type of tool pin profile produces good material stirring quality and mixing of dissimilar plasticized metals during welding. Square type of tool pin profile produces insufficient mixing of dissimilar plasticized metals because tool pin is incapable of deforming appropriate metal during rotation leads to low micro hardness. Similar results have been investigated by Rajkumar et al. [19].

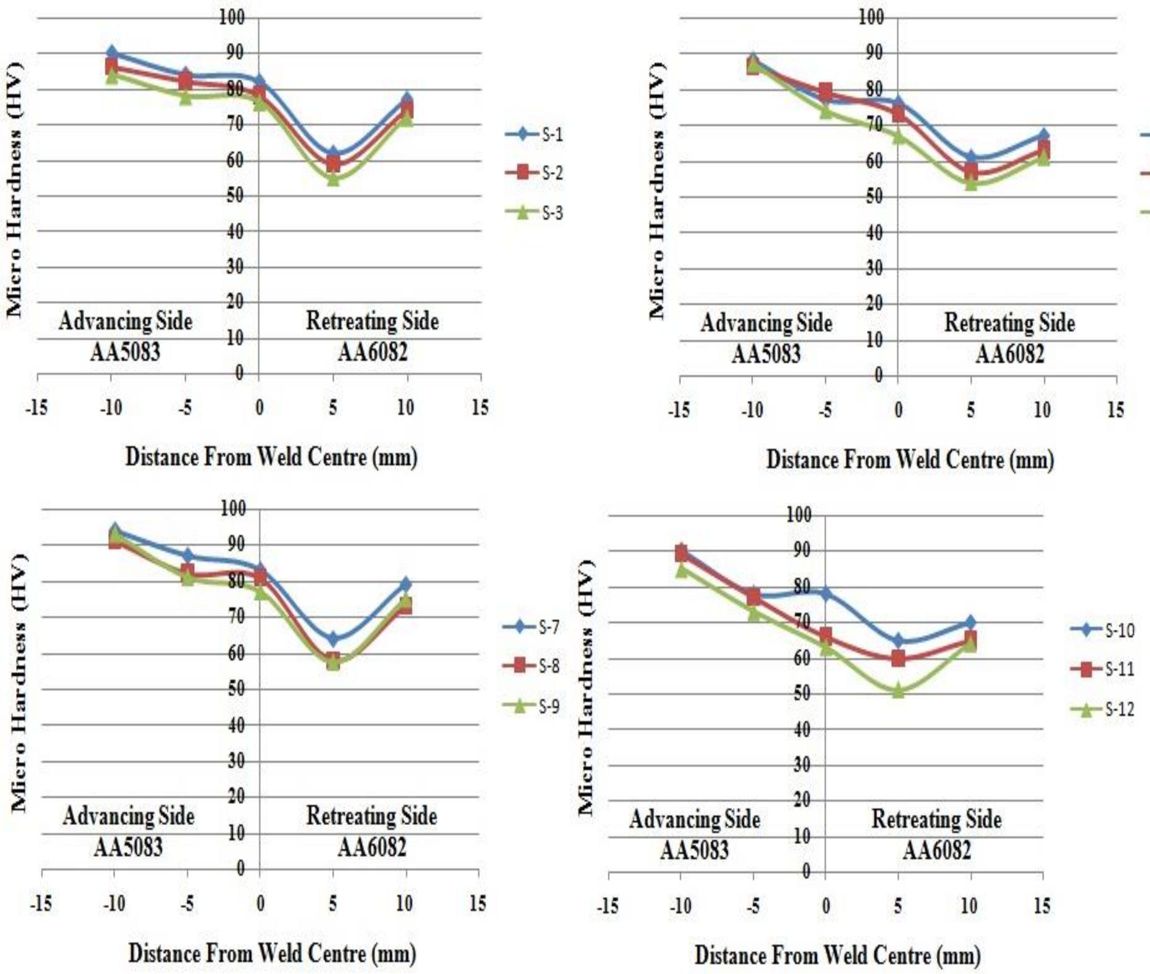

Fig. 5. Effect of Tool shape and welding parameters on Microhardness variations across friction stir welded joints.
(full colour version available online)

3.3 Microstructure Analysis

Thermal and mechanical stresses caused by tool stirring and axial force resulted in the formation of weld nugget zone (WZ), thermo mechanically affected zone (TMAZ) and heat affected zone (HAZ) in friction stir welded joints. On the basis of the results obtained during mechanical characterization, the best parameters were selected and microstructure evaluation was carried out on specimens welded using chosen parameters. The micrographs of the centre of weld nugget zones, thermo mechanically affected zone and heat affected zone for material welded using speed of 20 $mm \cdot min^{-1}$ and tool rotational speed of 1200 rpm with straight cylindrical tool pin profile are shown in Fig. 6. The microstructure of aluminum alloys joined by FSW was studied by employing optical microscopy at 100 µm. Images of weld zones cross section when AA5083 is kept in the advancing side and AA6082 is kept in the retreating side are outlined. The weld nugget zone showed proper material mixing because of severe plastic deformation and high temperature sufficient to cause dynamic recrystallization which was caused by rotation and traversing of FSW tool during welding. Therefore, the coarser grain structure of the base material is transformed into the fine and equiaxed grain structure in weld nugget.

Changing the welding speed and tool rotational speed have significant effect on the flow of the material within the stir zone. The extent of mixing and interface disruption increases as the tool rotational speed was increased and the welding speed was decreased.

The rubbing of the tool shoulder on the plate material creates frictional heat. The rotary action of the tool leads to stirring and mixing of plasticized material around the tool pin. As a result, the welds produced with tool rotational speed of 1200 rpm and welding speed of 20 mm·min^{-1}exhibited the formation of onion ring and superior material mixing. When the tool rotational speed increases, the quantity of plasticized material and material transportation from advancing side to retreating side increases. Our results are in the agreement with those found by Park et al. [20].

In friction stir welding the heat generation is due to the rubbing of the tool on work piece and the plastic deformation of the material. Tool pin profile has a remarkable effect on the rubbing and the effect on the welded material plastic deformation. The microstructure of the dissimilar aluminum alloy joints prepared by friction stir welding by straight cylindrical threaded pin profile at rotational speed of 1200 rpm and welding speed of 20 mm·min^{-1} is shown in Fig. 6. From the investigations, it was found that the joints fabricated by cylindrical threaded pin tool are defect free and onion ring are observed in the weld nugget zone. It was also found that the tool having straight cylindrical threaded tool profile causes larger plastic deformation to make more plasticized materials due to stronger stirring actions during FSW. Threaded cylindrical pin yielded the defect free joints. This may be yielded due to proper flow of plasticized material around the tool pin during stirring. In case of square pin profile the deformation included heat generation during the welding is marginally insufficient compared to cylindrical threaded pin profile.

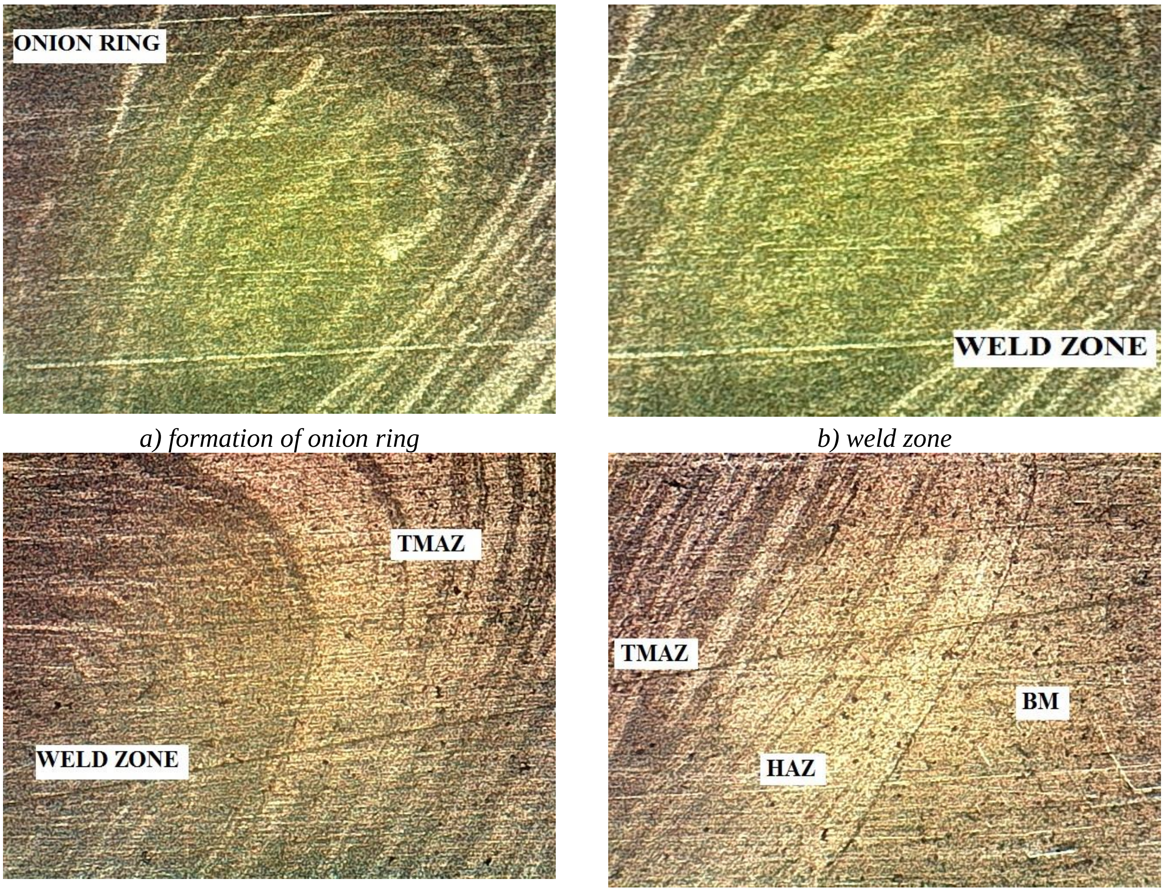

a) formation of onion ring *b) weld zone*

c) transition from weld zone to TMAZ *d) transition from TMAZ to BM.*

Fig. 6. Microstructure of various regions in weld zone using straight cylindrical threaded pin profile at welding speed of 20 mm·min^{-1} and rotational speed of 1200 rpm (AA5083-AS, AA6082-RS).

(full colour version available online)

4. Conclusion

In the present work the effect of tool shape and welding parameters on the microstructure and mechanical properties of dissimilar friction stir welded aluminum alloys AA5083 and AA6082 were investigated. The results can be summarized as follows:

- At low welding speed and high tool rotational speed, the joints exhibited satisfactory tensile strength and micro hardness. Joints prepared by low welding speed (20 mm·min^{-1}) and high rotational speed (1200 rpm), resulted in high heat input provided microstructurally and mechanically better joints.
- Friction Stir Welding tool with two different pin profiles suitable for dissimilar frictions stir welding of aluminum alloys were fabricated. Straight cylindrical threaded pin profile is preferred over square pin profile due to the superior performance of the joints.
- Maximum tensile strength of the joint of 121 MPa was achieved at low welding speed of 20 mm·min^{-1} and high tool rotational speed of 1200 rpm, when straight cylindrical threaded pin was used.
- The temperature field in dissimilar FSW of AA5083 and AA6082 is distributed asymmetrically producing larger thermally affected region in the heat treatable aluminum AA6082 alloy.
- Welded materials were more properly mixed and onion ring structure was formed at lower welding speed and higher rotational speed.

References

[1] A. Handa, V. Chawla: Mater. Eng. – Mater. Inž. 20(3) (2013) 102-111.

[2] A. Handa, V. Chawla: Int. J. Adv. Manuf. Tech. 75(9-12) (2014) 1493-1500.

[3] G. Casalino, S. Campanelli, M. Mortello: Procedia Engineering 69 (2014) 1541-1548.

[4] T. Hirata, T. Ogur, H. Hagin, T. Tanaka, S.W. Chung, Y. Takigawa, K. Higashi: Mater. Sci. Eng. 456(1) (2007) 344-349.

[5] W. Xu, J. Liu, H. Zhu, L. Fu: Mater. Des. 47 (2013) 599-606.

[6] P. Cavaliere, A. Squillace, F. Panella: J. Mater. Process. Technol. 200(1) (2008) 364-372.

[7] R. Palanivel, P.K. Mathews, I. Dinaharan, N. Murugan: Trans. Nonferrous Met. Soc. China 24 (2014) 58-65.

[8] I. Dinaharan, K. Kalaiselvan, S.J. Vijay, P. Raja: Arch. Civ. Mech. Eng. 12(4) (2012) 446-454.

[9] K. Kumar, S.V. Kailas: Mater. Sci. Eng. A485(1) (2008) 367-374.

[10] S. Rajakumar, C. Muralidharan, V. Balasubramanian: Mater. Des. 32 (2011) 535-549.

[11] B.T. Gibson, D.H. Lammlein, T.J. Prater, W.R. Longhurst, C.D. Cox, M.C. Ballun, K.J. Dharmaraj, G.E. Cook, A.M. Strauss: J. Manufacturing Processes 16(1) (2014) 56-73.

[12] H.J. Aval, S. Serajzadeh, A.H. Kokabi: J. Mater. Sci. 46(10) (2011) 3258-3268.

[13] M. Yuqing, K. Liming, L. Fencheng, L. Qiang, H. Chunping, L. Xing: Mater. Des. 62 (2014) 334-343.

[14] S.A. Khodir, T. Shibayanagi: Mater. Sci. Eng. B 148 (2008) 82-87.

[15] C. Sharma, D.K. Dwivedi, P. Kumar: Mater. Des. 36 (2012) 379-390.

[16] M. Ilangovan, S.R. Boopathy, V. Balasubramanian: Defence Technology 11(2) (2015) 174-184.

[17] W. Tang, X. Guo, J.C. McClure, L.E. Murr, A. Nunes: J. Mater. Process Manuf. Sci. 7(2) (1998) 163-172.

[18] B. Gungor, E. Kaluc, E. Taban, A. Sik: Mater. Des. 56 (2014) 84-90.

[19] V. Rajkumar, M. VenkateshKannan, P. Sadeesh, N. Arivazhagan, R.K. Devendranath: Procedia Engineering 75 (2014) 93-97.

[20] S.K. Park, S.T. Hong, J.H. Park, K.Y. Park, Y.J. Kwon, H.J. Son: Sci. Tech. Welding Joining 15(4) (2010) 331-336.

EVALUATION OF HVOF COATINGS

Landová Mariana[1,*], Janette Brezinová[1]

[1] Technical University of Košice, Faculty of Mechanical Engineering, Department of Technology and Materials, Mäsiarska 74, 04001 Košice, Slovak Republic

[*]corresponding author: Tel.: +421 55 602 3519, e-mail: mariana.landova@tuke.sk

Resume

Attention in this paper is devoted to the evaluation of wear coatings deposited using HVOF technology (high velocity oxy-fuel). There were evaluated three types of coatings based on WC-Co (next only 1343), WC-Co-Cr (next only 1350) and Cr_3C_2-25NiCr (next only 1375). There was assessed adherence of coatings, micro hardness, porosity and the tribological properties of erosive, abrasive, adhesive and wear resistance of coatings in terms of cyclic thermal load. Thanks to wide variety of suitable materials and their combinations, the area of utilization thermally sprayed coatings is very broad. It is possible to deposit coatings of various materials from pure metals to special alloys. The best results in the evaluated properties were achieved at the coating with the label 1375.

Article info

Article history:
Received 20 June 2015
Accepted 05 May 2016
Online 10 July 2016

Keywords:
HVOF technology;
Tribological properties;
Porosity of coatings;
Erosive wear;
Adhesive wear;
Abrasive wear.

Available online: http://fstroj.uniza.sk/journal-mi/PDF/2016/09-2016.pdf

ISSN 1335-0803 (print version)
ISSN 1338-6174 (online version)

1. Introduction

Coatings applied by technology HVOF (High Velocity Oxygen Fuel) belong among the dynamically developing areas. In view of their excellent properties such as high resistance to heat, corrosion and wear are used in the basic industry as well as in renovation. During spraying the minimum thermal changes of the substrate occurs. The surface roughness of the base material with a surface treatment of these coatings is low [1]. Thermal sprayed coatings are widely used in applications on different surfaces to reduce the wear and increase their resistance to corrosion. Aviation, automotive, textile and mining industries are one of the many areas of the usage of thermally sprayed coatings, where are used for the different advantages that this group of coatings offer [2].

Progressive methods of thermal spraying include: thermal spraying by plasma, thermal spraying and explosion spraying high flame - HVOF (high velocity oxy-fuel). HVOF is a technological process of coating application, where the microparticles are of metal alloy or cermet, driven and heated in sonic or supersonic stream of gas and deposited on a substrate at high speed to form a thin layer of melted metal [3].

The process of coating application represents the most modern methods of thermally sprayed metal powders. It uses a combination of fuel-karosen that burn with plenty of oxygen and produce a flame, which combines a relatively low melting temperature of about 3000 ° C with extreme speed up-to 2000 m·s-1. It results in extremely dense, well bonded coatings with little or no oxidation during application [4, 5].

These technologies are the subject of studies dealing with the optimization of process parameters consistently bringing good bond strength with minimal residual stresses and low porosity. Today, these high-quality coatings commonly used [5].

Table 1

Chemical composition of the steel substrate (wt. %) [6].

C	Mn	Si	P	S
0.12 – 0.18	0.30 – 0.60	0.15 – 0.40	Max. 0.035	Max. 0.035

Table 2

Chemical composition of the powders (wt. %) [7].

Powder	C	Co	Fe	W	Cr	Ni
WC – 17 Co (1343)	5.5	16.2	0. 036	78.4		
WC-Co-Cr (1350)	5.5	9.9	0.02	80.58	3.9	
Cr_3C_2-25NiCr (1375)	10				68.5	21

2. Materials and experimental methods

The base material was used carbon steel C15E (STN 41 2020, 1.1141). Chemical composition of the steel is listed in Table 1 [6]. The substrates for test samples were of cylindrical shape Ø 50 mm, height of 15 mm. Test samples were pre-treated by air grit blasting: air pressure of 0.5 MPa, shot media - brown corundum, grain size 1.00 mm.

2.1 Technology of application coatings

Thermal spraying techniques are coating processes in which melted (or heated) materials are sprayed onto a surface. The "feedstock" (coating precursor) is heated by electrical (plasma or arc) or chemical means (combustion flame). The coatings were applied by HVOF technology. On the spray coating was used PRAXAIR Tafa JP 5000 device with the system HP / HVOF as powder feeder HVOF System Powder Feeder 1264.

2.2 Material of coatings

There were deposited three types of coatings by HVOF technology on pre-treated samples. On the first group of samples, coating of 1343 (C-17Co) was applied, on the second group of samples coating of 1350 (WC-Co-Cr) was deposited and on the third group of samples coating 1375 (Cr3C2-25NiCr) was deposited. Materials of coatings were supplied as a powder, agglomerated and sintered, produced by Praxair, Inc., USA. Table 2 shows chemical composition of the powders [7].

2.3 The test parameters

To determine the basic properties of coatings "as-sprayed" and after thermal cycles were used these methods:

Assessment methodology microhardness of coatings: microhardness was measured according to STN ISO 4516 on Shimadzu HMV-2E test equipment, load 980.7 mN (10 g), dwell time 15 s [8].

Coating thickness: coating thickness measurements were carried out by means of QuaNix Keyless device. This device permits measuring the thickness of non-magnetic coatings on ferrous materials for example: lacquers, enamels, plastics, anodizing, and all the insulating layers, and the non-conductive non-magnetic coatings on metallic substrates such: aluminum, copper, brass, bronze, etc. [9].

Thermal loading: Samples were subjected to cyclic thermal load in an electric chamber furnace according to the following schedule [8]:

- heating to 900 °C,
- dwell in the furnace for 20 minutes,
- cooling of samples in still air to ambient temperature.

Samples were subjected to 10 thermal cycles, and after the 3rd, 5th, 8th and 10th thermal cycle.

Porosity of coatings was determined by mercury porosimetry using PoreMaster porosimeter [7].

The adhesion of the coating was evaluated by pull-off test according to STN EN 582 with help of tensile machine ZDM 10/91. After pull-off adhesion test, tensile stress necessary to rupture the weakest inter-phase (adhesive fracture) or the weaker component (cohesive fracture) of the test arrangement and also the nature of fraction were evaluated [8].

Erosive wear of the coatings: the coatings were subjected to erosion wear in abrasive impact angles 45° and 75°. To simulate the process of oxide impact a laboratory mechanical blasting device was used, which allows monitoring the circulation of abrasive. Abrasive used - brown corundum (Al_2O_3), grain size 1 mm. Intensity of coatings wear was evaluated using gravimeter (mass loss of the coating). Peripheral speed of blasting wheel was 51.0 m.s^{-1} and output speed of abrasive was 70.98 m.s^{-1}. One erosive cycle means application of 500 g abrasive by abrasive grit blasting technology [8].

Adhesive wear: to simulate the working conditions, coatings were subjected to adhesive wear using pin-on-disc test (ISO 20808) at 21 °C and 900 °C. Testing conditions: relative humidity 21 %, atmosphere: air, test ball diameter Ø 6 mm, radius of ball track was 5.01 mm, linear velocity 10.00 cm·s^{-1}, and normal load 5 N, stop condition 300 m [7].

Abrasive wear: abrasion resistance of coatings was evaluated on the device. The principle of the test is to be wading in bulk abrasives. Used abrasive was a brown aluminum oxide with grain size 1.2 mm, speed of the sample in abrasive was 1.74 m.s^{-1}, where *n* (turn) is 123 min^{-1}, dive into abrasive samples was 60 mm. Samples were subjected to impact abrasive at angles 45° and 75° [10].

3. Results and discussion

Thickness of the coatings as sprayed, were as follows: 1 343 – 234 μm, 1 350 – 356 μm and 1 375 – 393 μm. It was made 12 measurements and subsequently measured value calculated the average thickness of the coating. The measurements are shown in the Table 3, depicts the results.

Microhardness of the coatings: measured values are in Table 4 and shown in Fig. 1. The highest microhardness values was shown by coating 1 350 (1 447 HV 0.1) which was caused by a high content of tungsten and addition of cobalt compared to the coating 1 343, which also contains tungsten but at lower concentrations and had lower values of microhardness (1010 HV0.1). The lowest microhardness values were shown in coating 1375 with a high content of chromium, tungsten-free (975 HV 0.1) [11].

Porosity: the assessment of porosity showed that coating 1350 is more porous compared to the other two coatings which have almost the same porosity considering the structure of a coating and its chemical composition. Table 5 shows the recorded values of total porosity coatings, graphical representation of measured results shown in Fig. 2.

Table 3

Thickness of coatings (μm).

Coating	The average value
1343	334.02
1350	356.30
1375	393.30

Table 4

Micro-hardness coating (HV 0,1).

coating	1345	1350	1375
the average value	1009.66	1390	1154

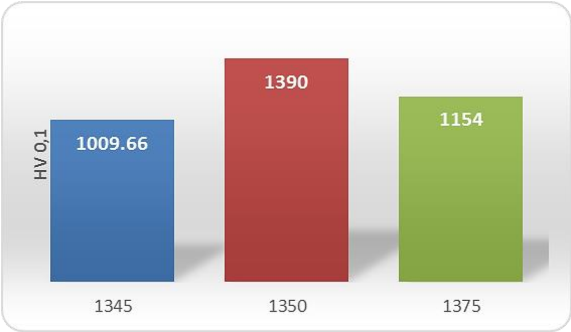

Fig. 1 Micro-hardness coating.
(full colour version available online)

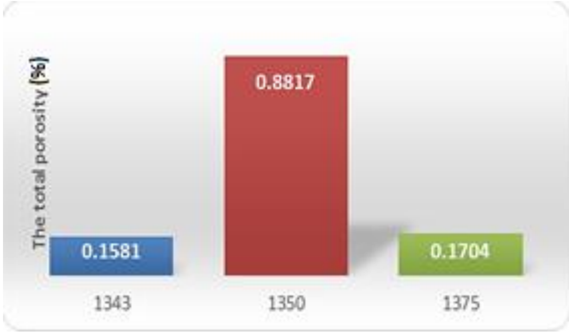

Fig. 2 Porosity coatings (%).
(full colour version available online)

Table 5

Porosity coatings (%).

Coating	„Total PS" [%]
1343	0.1581
1350	0.8817
1375	0.1704

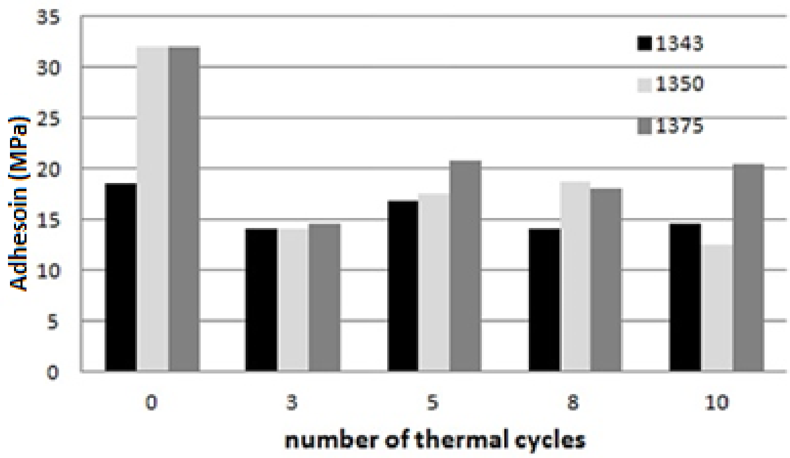

Fig. 3. Adhesive wear of coatings after thermal cycles.

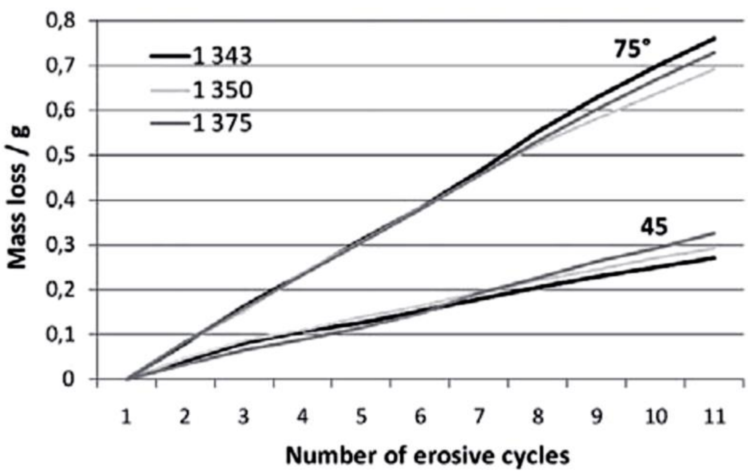

Fig. 4. Erosive wear of the coatings [4].

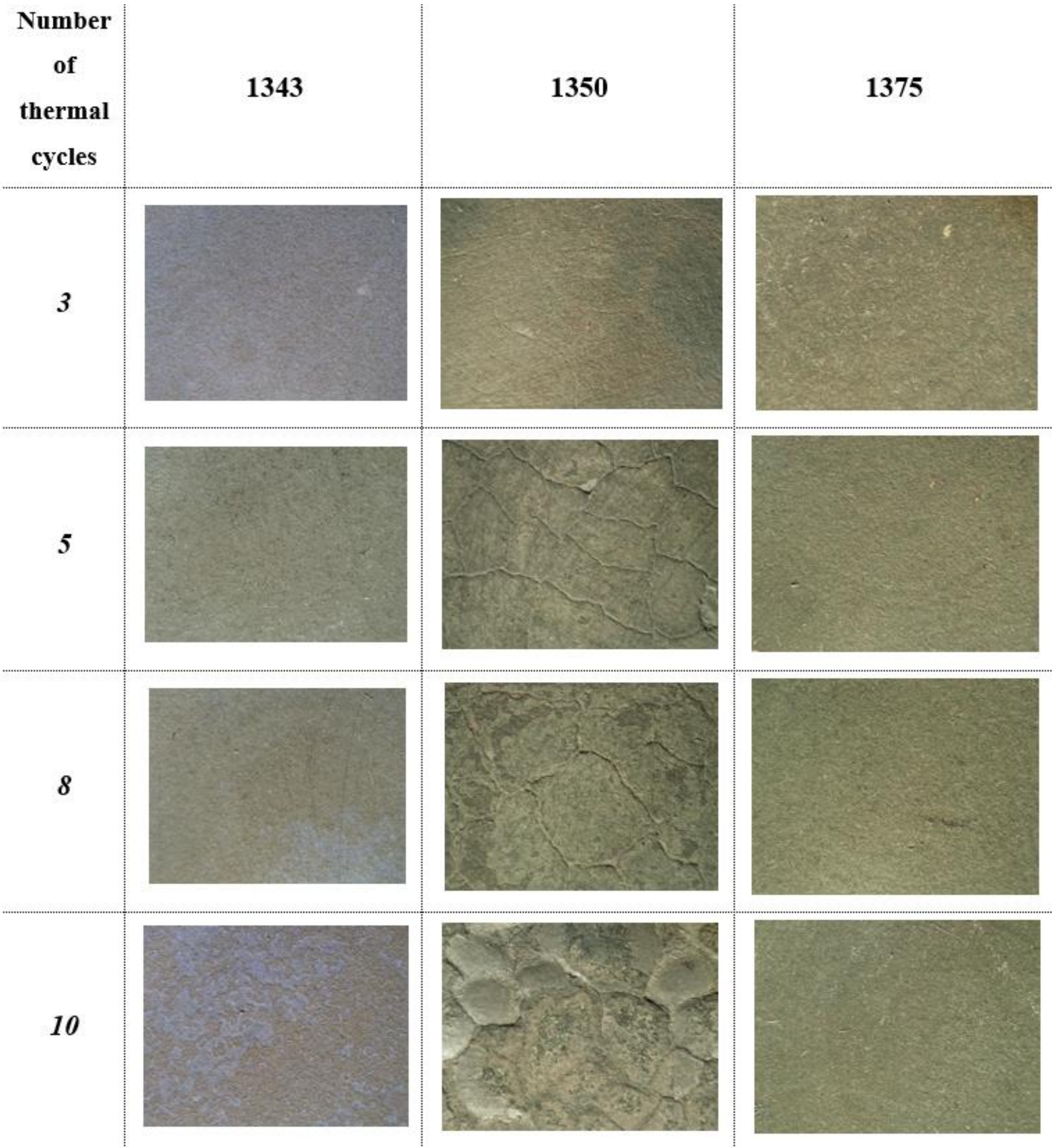

Fig. 5. Appearance of surfaces of investigated coatings after thermal cyclic loading [8].
(full colour version available online)

3.1 Evaluation of tribological tests

Adhesive wear: Results of coatings wear test at 900 °C showed that the wear rate of coatings 1343 and 1375 is extremely small, just a roughness change in wear track occurred. The coating 1350 showed small removal of material, Vdisc, 900°C = 0.056 mm^3, Wdisc, 900°C = $3.7.10^{-5}$ $mm^3 \cdot N^{-1} \cdot m^{-1}$. For other coatings was not observed measurable weight loss of coating material. Results of coatings adhesion are shown in Fig. 3. [7].

The measured values of the adhesion of coatings as-sprayed and the type of fracture showed that in neither case the damage of the coating occurred, therefore the observed initial adhesion values do not correspond to the actual adhesion of coatings, which is definitely higher [8].

Erosive wear: Fig. 4 depicts the dependence of erosive wear on the different impact angles of abrasive. For all types of coatings very similar dependences were achieved. Higher weight losses were recorded at an impact angle of 75° in all types of coatings. The references show that for the harder material, which also the evaluated coatings belong to, more intensive wear occurs at a larger impact angles, as confirmed by experiment [11].

Abrasive wear: Values of abrasion coatings were measured at angles of impact of bulk abrasive 45° and 75°. The highest value was recorded at both angles impact on coating 1343. At the same time, when compared angles of impact of this coating we conclude that greater weight wear was recorded at an angle of 45°. On 1350 and 1375 coatings were not measured weight losses [10].

Thermal loading: Despite its high hardness, the coating 1350 suffered thermal cracking after 3 thermal cycles, the surface of coating 1343 covered with a layer of blue oxides and showed strong chalking during the thermal cyclic loading. The coating 1375 retained its aesthetic and tactile qualities after thermal cycles. The appearance of surfaces of coatings during thermal cyclic loading is shown in Fig. 5 [8].

4. Conclusion

Experimental results point to the fact that, taking into account the results of measurements of resistance to cyclic heat such assessment shall be as follows: 1343 coating exhibits as said blue color with intense powdery, which was present throughout the course of cyclic thermal load. This activity can cause significant weight loss - coating thickness which may result in a lower life. Coating 1350 is also not suitable for real applications because of significant cracking, which leads to disruption of barrier protection effectiveness of the coating after a few cycles. This coating achieves high porosity value. In terms of follow-loading coatings primarily in corrosive conditions poses a risk just Sheetfed respectively. Open pores, which represents an input path for corrosive environments and for penetration into the coating degradation factors respectively. Thus delamination of the coating can occur, leading to the reduction and subsequent loss of adhesion of the coating. Penetrating corrosive atmosphere causes a reduction in the strength of cohesion coatings. Experimental studies confirmed low, almost zero porosity, in the 1375 coating when the HVOF technology was used for deposition. This claim was accepted on the basis of experimental evaluation, and despite the lower hardness, the coating has proven better in retaining the integrity, adherence, intractability or subject chalking throughout the thermal cyclic loading.

Acknowledgements

The article was drafted in resolving the grant VEGA 1/0600/13 - Research and development of advanced composite coatings and films for innovation engineering products.

Note

The shorter version of this research was presented at the SEMDOK 2015 International Seminar, 28. – 31. January, 2015, Terchová, Slovak Republic.

References

[1] T. Sahraouia, S. Guessasmab, M. A. Jeridanea, M. Hadjia: Mater. Des. 31(3) (2010) 1431 – 1437.

[2] M. Li, P. D. Christofides: Chem. Eng. Sci. 61(19) (2006) 6540-6552.

[3] V. A. D. Souza, A. Neville: Wear 259 (2005) 1-6.

[4] L. Thakura, N. Arora: Appl. Surf. Sci. 258(3) (2011) 1225–1234.

[5] W. Żórawski: Surf. Coat. Tech. 220 (2013) 276-281

[6] J. Brezinová, A. Guzanová, M. Egri: Chemicke listy 106(S3) (2012) 383-386.

[7] J. Brezinová, A. Guzanová, D. Draganovská1, M. Egri: Acta mechanica et automatica 7(3) (2013) 135-139.

[8] J. Brezinová, A. Guzanová, I. Mamuzić: Acta Metallurgica Slovaca 12(1) (2012) 20-27.

[9] J. Viňáš, M. Ábel, M. Jakubov: Transfer inovácií 15 (2009) 175-183.

[10] M. Egri: Možnosti zvyšovania životnosti strojných súčastí implementáciou nových renovačných technológii: Dissertation thesis (*Possibilities of increasing the life of machine parts renovation by implementing new technologies*), Košice: TUKE, 2013 (*in Slovak*).

[11] J. Brezinová, A. Guzanová: Metalurgija 51(2) (2012) 211-215.

THE VARIABLE CONTACT PRESSURE INFLUENCE ON THE TENSILE FORCE IN THE PROCESS OF STRIP SLIDING IN THE FLAT DIE IN IRONING

Milan Djordjević[1], Srbislav Aleksandrović[1], Vukić Lazić[1], Dušan Arsić[1], Ružica Radoslava Nikolić[1,2,*], Branislav Hadzima[2]

[1] Faculty of Engineering, University of Kragujevac, Sestre Janjić 6, 34000 Kragujevac, Serbia
[2] Research Center, University of Žilina, Univerzitna 1, 010 26 Žilina, Slovak Republic

[*]corresponding author: e-mail: ruzicarnikolic@yahoo.com

Resume

Possibilities to influence the deep drawing process during its duration are limited and generally consist of influences at the flange of the thin sheet, mainly by the contact pressure (the blank holding force). The common characteristics of previous investigations were setting of the fixed values of the blank holding force or the holder's pressure within the ironing tool. The objective of this investigation was the continuous setting of the variable pressure during the sliding process, via the preset functions, in order to analyze the variable pressure influence on the ironing process.

This is why an experimental computerized device was designed and constructed for analyzing the influence of the variable contact pressure on the sliding process of the model strip during the flat-die test. The multi-parameter experiment was conducted; various materials of the tested pieces were applied (primarily thin sheet made of Al alloys and low-carbon steels sheet, with and without coating); different versions of the tool's contact elements were used, with various friction regimes and influential parameters (variable contact pressure during the sliding process, etc.). This experimental device practically represents a simulator for realization and studying of the physical model of an important segment of the ironing process in the completely realistic conditions (materials, tools, etc.).

The aim was to find the optimal combination of the variable contact pressure and the tribological parameters, so that the punch force, as one of the process output parameters, would have the minimal value, as well as to avoid the undesired effects during the forming (difficult sliding of the flange, appearance of thin sheet's wrinkling, structural destruction, etc.).

Understanding the mutual dependence of the holder's variable pressure and other influences should enable improvement of the ironing process control and should contribute to better understanding of the phenomena occurring at the thin sheet's flange.

Available online: http://fstroj.uniza.sk/journal-mi/PDF/2016/10-2016.pdf

Article info

Article history:
Received 05 February 2016
Accepted 05 April 2016
Online 10 July 2016

Keywords:
Flat-die test;
Deep drawing;
Ironing;
Tribological model;
Contact pressure;
Punch force.

ISSN 1335-0803 (print version)
ISSN 1338-6174 (online version)

1. Introduction

Possibilities to influence the deep drawing process during its time of conducting are limited. They are reduced to influence on the thin sheet flange, mainly through the contact pressure (the blank holding force) and by action of the draw beads on the holder. The characteristics common to all the previous investigations in this field were setting of the fixed values of the blank holding force or the holder's pressure within the ironing tool. The objective of this investigation was continuous setting of the variable pressure during the sliding process, via the preset functions, in order to analyze the variable pressure influence on the ironing process, as well as other influences (die, contact conditions, material, etc.).

Influence of the variable contact pressure in the ironing process represents a very interesting current topic of research with the aim of discovering the new possibilities for control of this process. This is why the physical-tribological models are being developed. The most present is the model of the strip sliding between the flat surfaces, investigated in numerous papers in this area [1 - 5]. The problems of the ironing process modeling at the flange between the flat contact surfaces of the holder were considered in those papers. The tribological models were formed in the completely real environment: material, tool and machine, contact conditions, etc. In the majority of investigations, researchers were monitoring the variation of the friction coefficient and the punch (deformation) force, by varying the mentioned real conditions in which the process is conducted. They were using the dies with surfaces of different roughness. Different contact conditions were realized, not only by varying the states of the dies contact surfaces, but also by application of several types of lubricants for ironing and thin sheets with various coatings (Al and steel sheets), as well. In addition, it is possible to vary the sliding speed of the strip [6, 7]. The objective of the majority of investigations was to control the output parameters of the ironing process. The tendency is to obtain the least values of the friction coefficient and the deformation forces, on one hand, while on the other to obtain the parts of the desired geometry, without defects on the flange (wrinkles) [8 - 10].

Fratini et al. in [1] presented experimental investigations of the friction coefficient during the sliding of the thin sheet strips. The measurement system for the data acquisition was relatively simple and it monitored the variation of the force at the strip during the sliding process. The device enabled application of strips made of different thin sheets, as well as the cylindrical tool made of various materials. It was possible to set different contact conditions depending on the applied lubricant, coating on the material and the tool, roughness, etc. The obtained results were reliable, applicable in the thin sheets ironing processes, with the similar schematics of sliding. Szakaly and Lenard [2] were using a massive constructed device with the large contact surface. The contact pressure had constant values within range 1 to 15 MPa. Only one regime of the mixed friction was realized while the tool roughness was varied. Results obtained for the friction coefficient dependences mainly confirmed the known influences. The friction coefficient decreases for the higher speeds and contact pressures. However, the higher roughness did not always result in increase of the friction coefficient values. Figueiredo et al. in [3] presented experimental investigation of the friction coefficient in thin sheets on the two models. Results show that the test by the crossed sliding produced the lower values of the friction coefficient and that the reason for that probably was somewhat higher value of the contact pressure. In addition, they noticed that the friction coefficient decreased with realized number of passes due to the running-in process of surfaces. Coello et al. [4] presented voluminous investigation of the effects of the strip sliding between the flat surfaces. The thin sheet was made of the high strength steel with zinc coating and roughness in the form of bumps. Due to such roughness, it was expected that micro-pockets of lubricant would be formed and maintained what would cause the more favorable lubricating conditions. Authors have determined dependences of the friction coefficient on the sliding speed and the contact pressure for various lubricating conditions. The friction coefficient was decreasing with increase of the sliding speed and pressure, but not with increase of the lubricant layer's thickness. Kalbarczyk et al. [5] were monitoring the variation of the friction coefficient in terms of the contact pressure, temperature and applied lubricants. Besides the expected influences, authors especially emphasized that the effect of lubricants was significantly lower in thin sheets with the aluminum coating. Manoylov et al. [6] were considering the possibility of solving the dry contact problems that arise when the lubricant film is not thick enough to prevent the contact between the working surfaces. For that purpose, they were using the simple elastic-plastic model whose results were compared to results obtained by the FEM modeling of the rough surfaces contacts. Kondratiuk and Kuhn [7] were considering the friction and wear behavior of coatings during the hot sheet strip drawing. They were comparing the friction coefficient and worn mass loss in coated strip drawing of two coating alloys – Al-Si and the Zn-Ni. The electro-plated Zn-Si after the heat treatment had higher mass loss, but the lower friction coefficient, while the Al-Si coated blanks had more aggressive wear behavior, i.e. the adhesive wear to the die. Ghiotti and Bruschi [8] were studying the tribological behavior of the DLC (diamond-like-carbon) coatings as solution to appearance of the dry contact between the blank and the tool surfaces. They concluded that in the lubricated conditions the type of coating does not significantly influence the friction coefficient. However, in the dry coating conditions only the DLC coating has the friction coefficient value lower than in the lubricated conditions. Lee, Keum and Wagoner [9] were modeling the friction caused by different lubricants and surface roughness by designing the sheet metal friction tester. They verified the validity and accuracy of their model by comparing the tribological parameters results, obtained by the model, to experimental measurements' results. Kirkhorn et al. [10] were studying the influence of the tool steel microstructure on the friction in sheet metal forming. They concluded that the direct correlation between the amount of carbides in different steels and the friction coefficient during the sheet forming could not be reliably established. Bachchhav et al. [11] were studying the influence of various types of lubricants on tribological phenomena during the ironing process and they have ranked the tribological parameters according to their influence of the metal forming. Kalbarczyk et al. [12] considered the influence of three different oils of the scuffing of the concentrated friction joints with the low-friction coated elements, by the four-balls scuffing test. They were studying the PVD (plasma-vapor-deposited) coatings and concluded that the coatings take the role of additives to the lubricants used in the process. Djordjević et al. [13, 14] were studying the influence of different lubricants types on the multi-phase ironing process, while Pena-Paras et al. [15] considered the properties of the nano-lubricants and their properties under the extreme pressure during the ironing process. Addition of copper or titanium nano-particle additives to various lubricants results in increase of the load-carrying capacity of those lubricants and of the seizure loads, as well.

2. Experimental equipment and conditions

The experimental device, which was developed for this research, represents a simulator for realization and studying of the physical model of an important segment in the deep drawing process in the completely real conditions. The structure of the device consists of the hydraulic, electrical and mechanical modules. The hydraulic module consists of hydraulic aggregate (the pump, reservoir, filter, regulatory valve and the three-position distributer with manual control) and it provides the necessary pressure. The electric module provides reliable power to all the components and programmed control of the hydraulic system, to realize the functional pressure variations. The mechanical module (Fig. 1a) is the part of the device, which realizes the pulling of the sample between the two contact elements. It is mounted on the hydraulic press, which provides the pulling action, while the pressure of the sliding elements is realized by the hydraulic module.

The two materials of the working pieces were applied in the form of thin strips made of the Al alloy and the low-carbon steel thin sheets. The contact elements were prepared in two versions (Fig. 1b, c); the two friction regimes were applied (lubricating grease based on MoS_2 and oil for deep drawing) and four functions of the contact pressure variation, which is being set simultaneously during the process.

a) mechanical part of the device

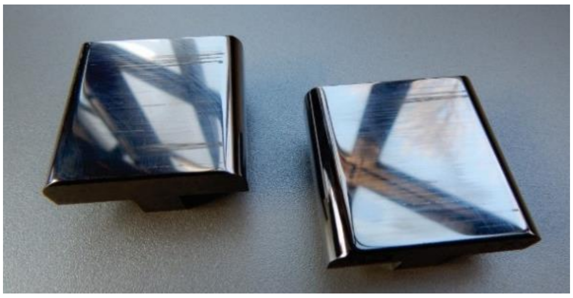

b) contact elements with polished surface

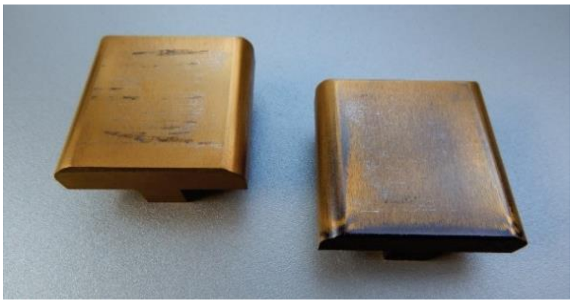

c) contact elements with the TiN coating.

Fig. 1. Mechanical part of the device with sliding elements.

(full colour version available online)

The pressure functions are predefined in advance and they are set by the electro-module (micro controller), which controls the hydraulic system (Fig. 2). The pressure is being set simultaneously during the drawing process and it is coupled with the pulling action provided by the hydraulic press. The setting time of functions is 180 s, what corresponds to the drawing step of 60 mm (Figs. 3 and 4).

3. Results and discussion

In Figs. 3 and 4 are presented graphs of the punch forces for samples made of the aluminum alloy and the low carbon steel thin sheets, for the four pressure functions shown in Fig. 2. The following conditions were applied for both materials' thin sheets: polished flat surfaces, the grease based on MoS_2 (Fig. 3), the TiN coating on the flat surfaces of the contact elements and deep drawing oil (Fig. 4). Besides the same conditions for both materials, there is a slight difference in the punch force values, though the trends on the curves are similar. There are somewhat higher values for all the contact pressure functions for the steel sheets. This could be explained by the better retaining of the lubricant on the aluminum sheets than on the steel one. In addition, the aluminum sheet is more deformable and it possesses better machinability than the steel sheets, thus the smaller punch forces are needed for its forming.

From both graphs in Fig. 3 one can notice that the highest values of the punch force were obtained by application of the pressure functions P2 and P3 (Fig. 2). The P2 function is of the increasing character and so is the P3 function up to the half of the step.

Increasing of the punch force worsens the sliding conditions, especially for the P2 functions, since the pressure gradually increases and it could squeeze out a large portion of the lubricant. For the P3 function, one could notice the prominent increase of the punch force in the first half of the step; with the pressure decrease in the second half the sliding conditions are improving and accordingly the punch force curve decreases. For the P1 and P4 functions, one could notice lower values of the punch force (Fig. 3a, b), what is a consequence of the decreasing character of pressure. The punch forces values thus show that it is better to start the process with the maximal pressure and then decrease it gradually during the drawing step (P1 and P4), than to start with the lowest pressure (P2 and P3) and then increase it gradually. One of the reasons for such behavior is the better retaining of the lubricant during the decreasing pressure phase, what was confirmed by experiments. The pressure curve P4 decreases more intensively in the first part of the step than the P1 curve during the whole step, thus the values of the punch force are lower for the P4 pressure curve.

In the second case are presented graphs of the punch force realized in somewhat different tribological conditions, (Fig. 4). The flat contact surfaces are coated by the titanium nitride (TiN) and as a lubricant the oil for deep drawing was applied. This oil, as it is known, has worse lubricating properties than the MoS_2 based grease. Those are the reasons that the significantly higher values of the punch forces were obtained for both strips, since sliding is more difficult. The high values of the contact pressure only augment the effect of the worsen lubricating by the oil. It possesses lower viscosity and density than the MoS_2 based grease, thus it can easier be squeezed out of the contact zone.

The highest values of the punch forces were obtained for application of the decreasing pressure function P1. It has the highest values of the contact pressure at the beginning of the step and at that moment the oil is squeezed out, what, as a consequence, has difficult strip sliding, even stopping (seizure). The P1 curve has the slow decreasing trend so the "braking" effect is being extended up to the half of the step, all the way to the point when the pressure reaches the value when the sliding becomes possible. The complete seizure results in thin sheet elongation, what could be concluded based on the punch force graph trend, which resembles the uniaxial tension diagram (P1, Fig. 4a, b). On the P2 and P4 punch force graphs one could notice the constant tendency at the beginning of the step, which could be explained by the strip skidding within the punch jaws, as a results of the difficult sliding. The punch force starts to increase from the moment when the blank holding force within the jaws supersedes the value that causes the constant pressure.

For the case of the P4 curve, the highest values of pressure at the beginning of the step are quickly superseded due to the more intensive decreasing trend (Fig. 2b) with respect to the P1 curve (Fig. 2a), thus as a results the difficult sliding does not occur and values of the punch force are very low during the large portion of the step (Fig. 4a, b). The punch force graph is completely in accordance with the pressure curve P4, i.e. the force has the lowest values at the portion of the step where the pressure is the least and the highest values at the beginning and at the end of the step. The P4 curve could be considered as the optimal pressure variation since the values of the punch force are the lowest of all the applied pressure functions, regardless of the fact that the lubricating is done by oil or the MoS_2 based grease. For the force graphs obtained by application of the P2 and P3 pressure functions the similar conclusions could be drawn for this case as for the case when lubrication was done with the MoS_2 based grease.

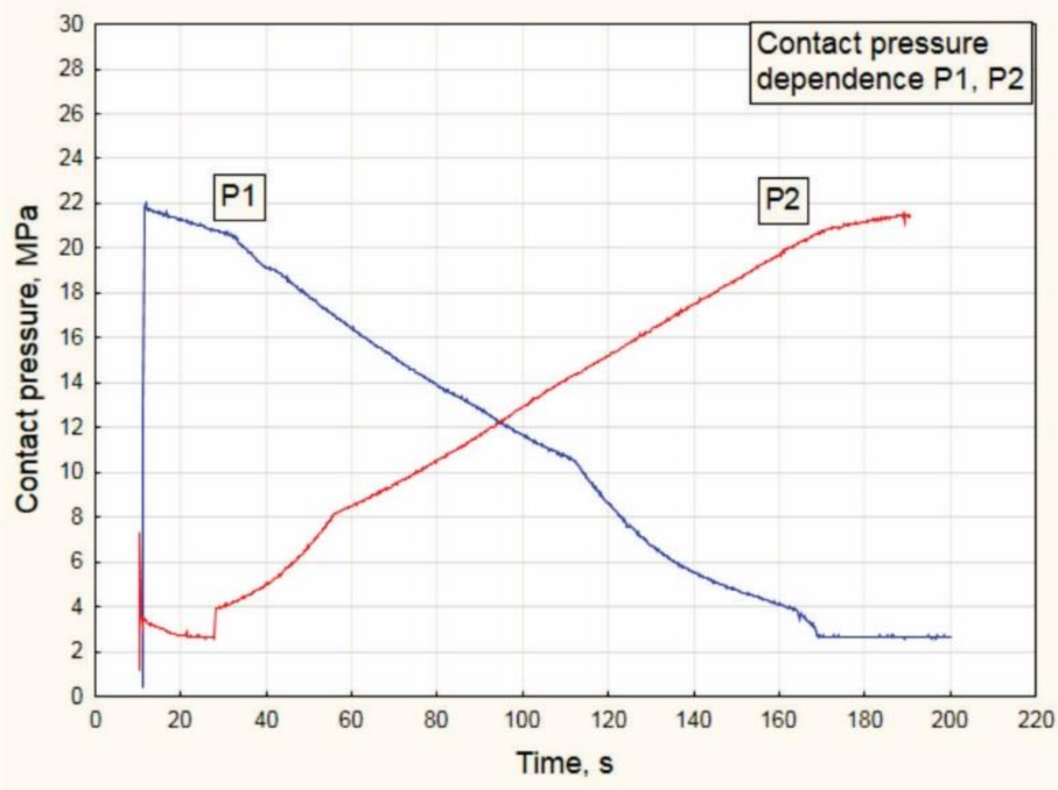

a) increasing (P1), decreasing (P2)

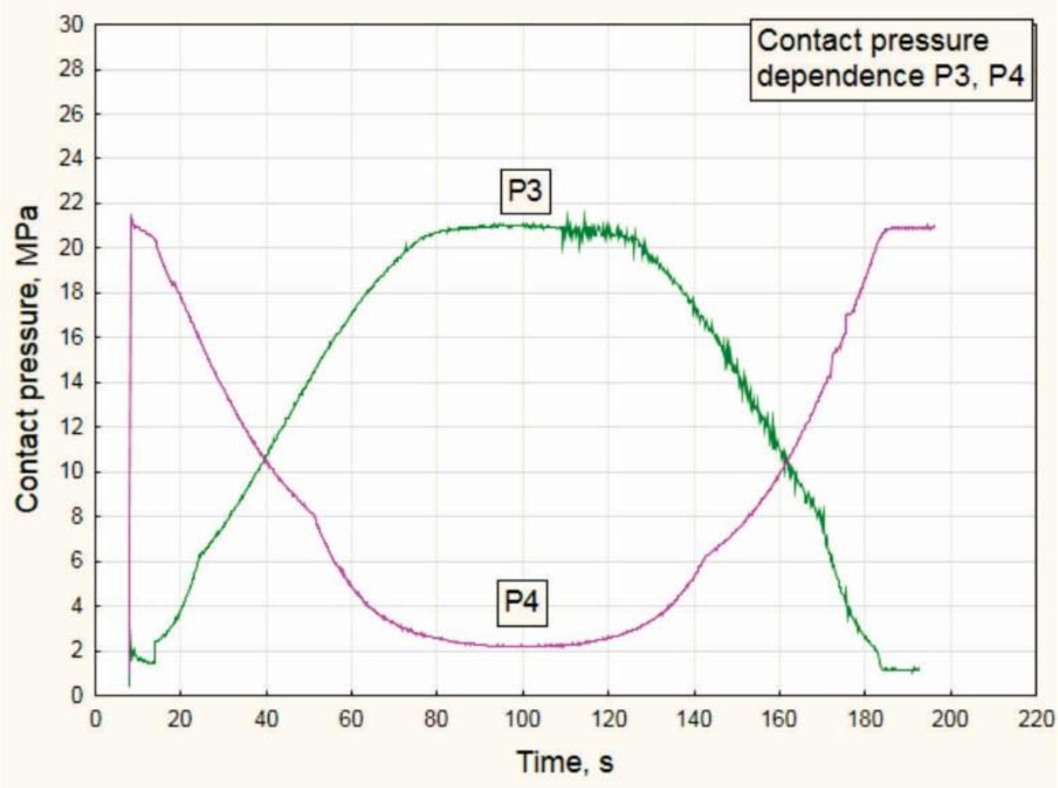

b) increasing-decreasing (P3) and decreasing-increasing (P4)

Fig. 2. Predefined functions of the contact pressure.

(full colour version available online)

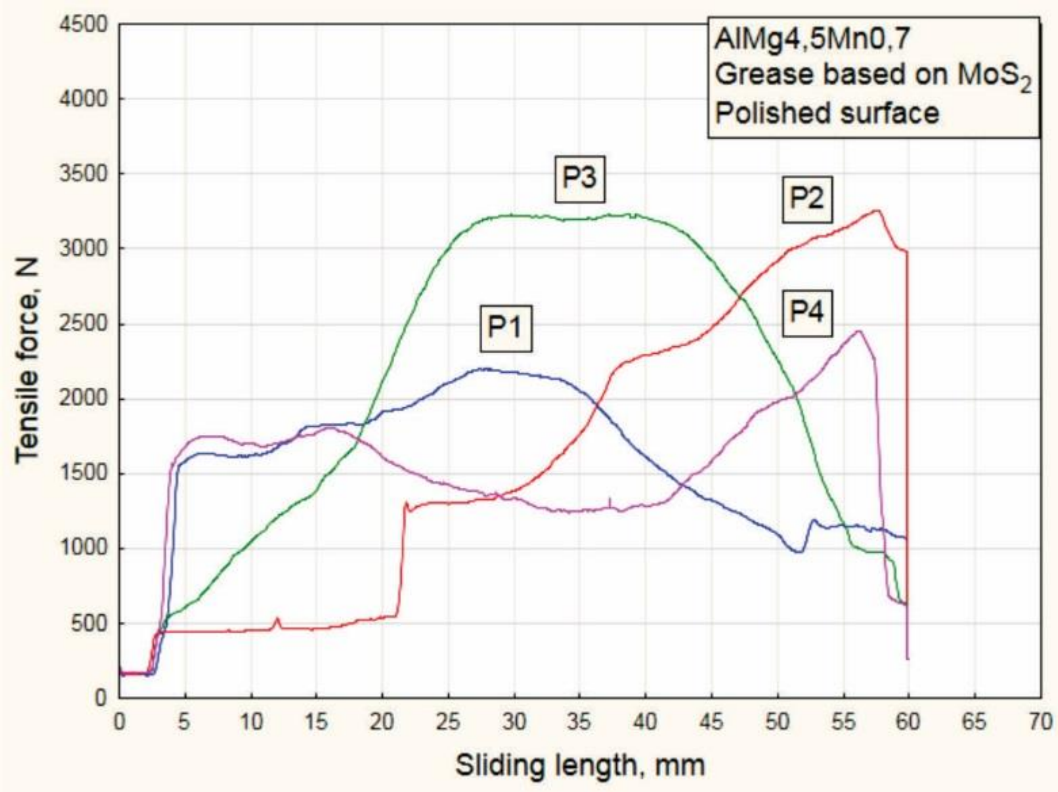

a) Al-alloy strip

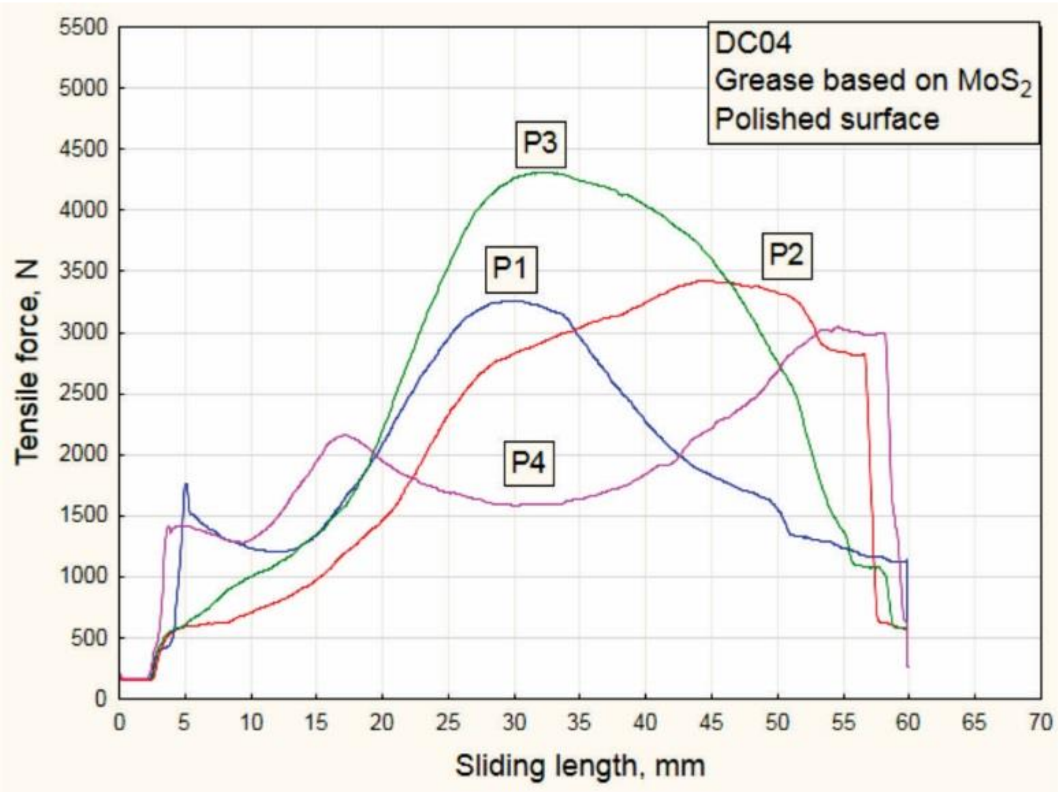

b) low-carbon steel strip

Fig. 3. The punch forces graphs for the strip sliding between the polished contact surfaces and the MoS2 based lubricating grease.

(full colour version available online)

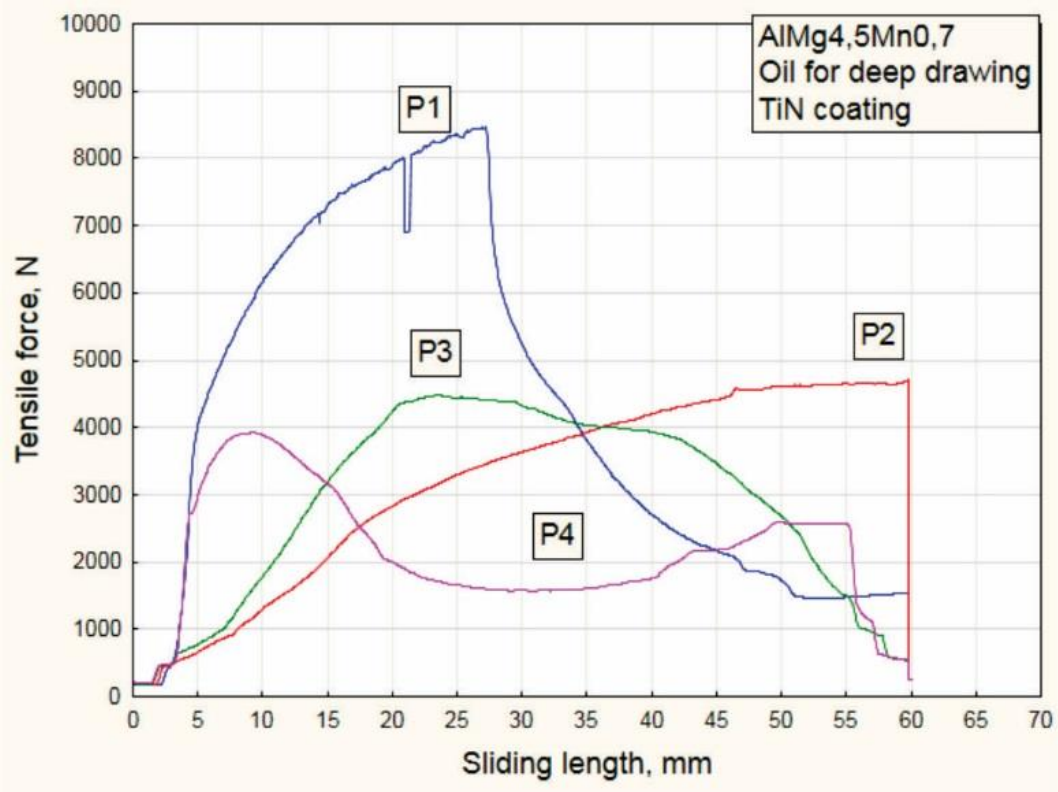

a) Al-alloy strip

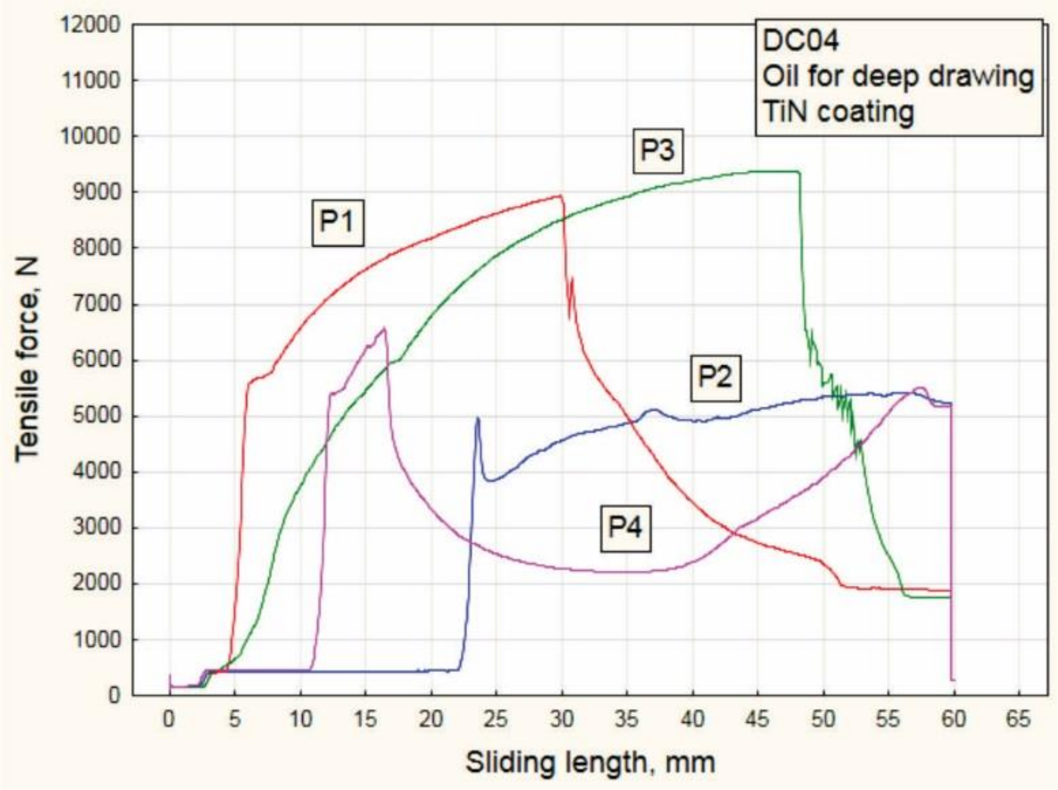

b) low-carbon steel strip

Fig. 4. The punch forces graphs for the strip sliding between the contact surfaces with the TiN coating and the deep drawing oil.

(full colour version available online)

4. Conclusion

Based on the conducted research, the following conclusions can be drawn:

a) Realization of this experimental apparatus and obtained results has the broader significance as the alternative approach in an area of the high technology. With the adequate changes in the mechanical part of the device, as well as in the control system, it is possible to investigate the influence of the drawing bead at the thin sheet flange, by setting the variable pressure;

b) The character of the punch force response shows that by the adequate combination of the simultaneous action of the contact pressure and the friction conditions one can influence the thin sheet forming process in a substantial and controlled manner;

c) The optimal combination of the tribological conditions and the variable pressure implies producing the tool's contact surfaces with the least roughness, application of the lubricant with good lubricating properties and the pressure variation with the more intensive decreasing trend in the first half of the step (P4). It is recommended to avoid the increasing pressure variation functions (P2 and P3), especially when the lubricant with worse properties is applied;

d) Application of the new materials, like the thin sheets made of the high strength steels, thin sheets with anti-corrosive coatings, stainless steel thin sheets, laminate and TWB thin sheets, etc. represents additional possibilities for using this apparatus in further investigations.

The presented results show that by the adequate selection of functional relation between the contact pressure and the tribological conditions one can successfully control the thin sheet sliding at the flange in the ironing process. In that way, it is contributed to better understanding of the material behavior at the flange and to minimizing the numerous problems that are accompanying this process in the real manufacturing conditions.

Acknowledgement

This research was partially financially supported by European regional development fund and Slovak state budget by the project "Research Center of the University of Žilina" - ITMS 26220220183 and by the Ministry of Education, Science and Technological Development of Republic of Serbia through grants: ON174004, TR32036, TR34002, TR35024 and TR33015.

Note

The shorter version of this research was presented at the SEMDOK 2016 International Seminar, 27. – 29. January, 2016, Terchová, Slovak Republic, reference [16].

References

[1] L. Fratini, S. L. Casto, E. L. Valvo: J. Mats. Process. Technol. 172(26) (2006)16-21.

[2] E.D. Szakaly, J.G. Lenard: J. Mats. Process. Techno. 210(30) (2010) 868-876.

[3] L. Figueiredo, A. Ramalho, M. C. Oliveira, L.F. Menezes: Wear 271 (2011) 1651-1657.

[4] J. Coello, V. Miguel, A. Martinez, F.J. Avellaneda, A. Calatayud: Wear 305 (2013) 129-139.

[5] A. Yanagida, A. Azushima: CIRP Annals-Manufac. Technol. 58 (2009) 247-250.

[6] A.V. Manoylov, M.J. Bryant, H.P. Evans: Tribology International 65(21) (2013) 248-258.

[7] J. Kondratiuk, P. Kuhn: Wear 272 (2011) 839-849.

[8] A. Ghiotti, S. Bruschi: Wear 271 (2010) 2454-2458.

[9] B.H. Lee, Y.T. Keum, R.H. Wagoner: J. Mats. Process. Technol. 130-131 (2002) 60–63.

[10] L. Kirkhorn, V. Bushlya, M. Andersson, J.E. Stahl: Wear 302 (2013) 1268-1278.

[11] B.D. Bachchhav, G.S. Lathkar, H. Bagchi: Indus. Lubrication and Tribology 66(6) (2014) 640-644.

[12] M. Kalbarczyk, R. Michalczewski, W. Piekoszewski, M. Szczerek: Eksploatacja

i Niezawodnosc – Maintenance and Reliability 15(4) (2013) 319-324.

[13] M. Djordjević, S. Aleksandrović, V. Lazić, M. Stefanović, R. Nikolić, D. Arsić: Mater. Eng.–Mater. Inž. 20(3) (2013) 147-152.

[14] M. Djordjević, D. Arsić, S. Aleksandrović, V. Lazić, D. Milosavljević, R. Nikolić: J. Balkan Trib. Assoc. 22 (2016) (in press).

[15] L. Peña-Parás, D. Maldonado-Cortés, J. Taha-Tijerina, P. García-Pineda, G. Tadeo, G. M. Irigoyen, J. Gutiérrez, D. Sánchez: Ind. Lubr. and Trib. 68(1) (2016) 30-34.

[16] M. Djordjević, S. Aleksandrović, R. R. Nikolić, V. Lazić, D. Arsić: In Proc. of Abstracts of "SEMDOK 2016" – 21st International Seminar, Terchova, Slovakia 2016, p. 10.

HIGH NITROGEN AUSTENITIC STAINLESS STEEL PRECIPITATION DURING ISOTHERMAL ANNEALING

Mária Dománková[1,*], Katarína Bártová[1], Ivan Slatkovský[1], Peter Pinke[2]

[1] Institute of Materials Science, Faculty of Material Science and Technology in Trnava, Slovak University of Technology in Bratislava, Bottova 25, 917 24 Trnava, Slovak Republic
[2] Óbuda University, Bánki Donát Faculty of Mechanical and Safety Engineering, Department of Materials Technology, 1081 Budapest, Népszínház u. 8. Hungary

[*]corresponding author: e-mail: maria.domankova@stuba.sk

Resume

The time-temperature-precipitation in high-nitrogen austenitic stainless steel was investigated using light optical microscopy, transmission electron microscopy, selected area diffraction and energy-dispersive X-ray spectroscopy. The isothermal precipitation kinetics curves and the corresponding precipitation activation energy were obtained. The diffusion activation energy of M_2N precipitation is 129 $kJ.mol^{-1}$. The results show that critical temperature for M_2N precipitation is about 825°C with the corresponding incubation period 2.5 min.

Article info

Article history:
Received 21 December 2015
Accepted 01 July 2016
Online 18 July 2016

Keywords:
Stainless Steel;
Annealing;
Sensitization.

Available online: http://fstroj.uniza.sk/journal-mi/PDF/2016/10-2016.pdf

ISSN 1335-0803 (print version)
ISSN 1338-6174 (online version)

1. Introduction

Nickel-free high nitrogen austenitic stainless steels (HN ASS) are highly attractive nowadays of their excellent mechanical and corrosion properties. They are also cheaper than nickel which has prospected possibility of allergic reactions in the human body. Also nickel is starting to be significantly deficient element what is also reflected in increasing prices of its alloys. Also the primary application of nickel is in jet engines [1 - 4], so in case of insufficient resources, manufacturing of stainless steels would have to be reduced in behalf of nickel alloys for aeronautic industry. The application field of nitrogen alloyed ASS is wide including power-generating industry, ship building, chemical equipment, biomaterials and petroleum industry. There are several attributes which makes the use of HN ASS favourable compared to the more conventional alloys. Some of these are high yield and tensile strength, high ductility, good strength fracture toughness combination, high strain hardening potential and favourable corrosion properties [5 - 7]. Generally austenitic stainless steels alloyed by chromium and nickel are considered as heat resistant up-to 800 °C [8, 9]. However, the excellent properties of HN ASS will be damaged if the precipitation of nitrides or other secondary phase occurs during thermal progress such as hot forming, heat treatment and welding [10, 11]. This means that HN ASS cannot completely replace Cr-Ni stainless steels, however in many applications they can be successfully used as a cheaper alternative and to save nickel, which is starting to be significantly deficit.

The purposes of the present study are to examine the morphology and the precipitation kinetics of M_2N precipitates in the isothermal annealing process and to provide some theoretical basis for the heat processes.

2. Experimental material and methods

The experimental steel with the chemical composition of Cr 21.0, Mn 23.0, N 0.85, C 0.04, V 0.2, Ni 1.5, Fe balance (in mass percent) was solution heat treated (1100° C/30 min. followed by water quenching) and then annealed in the temperature range from 650 to 900° C for holding time 5 min. to 30 hours.

The specimens for light optical microscopy (LOM) examination were polished up to fine diamond (~1μm) finish. The specimens were etched chemically for 60 sec. using solution: 10 ml H_2SO_4 + 10 ml HNO_3 + 20 ml HF + 50 ml distilled H_2O. Then the screening of microstructures was done using a light microscope NEOPHOT 32 equipped with the CCD camera. Quantitative metallographic software adopted to measure the percentage of precipitates.

For the individual secondary phase identification transmission electron microscopy (TEM) of the dual stage replicas was utilised. Thin foils suitable for TEM observation were prepared from each of the samples. Small discs of 3 mm in diameter and thick about 0.1 mm were jet-electropolished in electrolyte HNO_3 : CH_3OH = 3 : 7, at 0°C and 15V to obtain transparent areas near the central hole. The jet-electropolishing was done by TENUPOL 5. TEM observations were performed using JEOL 200 CX operated at 200 kV and Philips CM 300 operating at 300 kV equipped with energy-dispersive X-ray spectrometer (EDX), which was used for the microchemical analyses. The analysis was supplemented by selected area electron diffraction (SAD) for the phases identification.

3. Results

Fig. 1a – 1d show microstructure of the experimental steel observed by light optical microscope (LOM). From the pictures is obvious the heterogeneity in the grain size of polyhedral austenitic matrix. The local precipitation at the grain boundaries was observed in the microstructure of samples annealed at 850°C/30 min. and 1 h, respectively (Figs. 1a and 1b). Fig. 1c shows microstructure of the sample annealed at 850°C / 10 h. The local precipitation at the grain boundaries is more intensive and there are some dark grains with lamellar shaped forms of discontinuous precipitation. The similar microstructure was observed in the case of the sample annealed at 850 °C / 30 h (Fig. 1d).

The detail of the grain boundary observed by TEM using replicas is show in Fig. 2a. The particles of the irregular shape were observed at the grain boundaries. These particles were identified as nitride M_2N using SAD (Fig. 2b). The chemical composition of nitride M_2N determined by EDX analysis is given in the Table 1.

Fig. 3a shows the bright-field image of the grain boundary serration observed by TEM using thin foils. The serration of grain boundary was caused by precipitation of nitride M_2N during annealing at 800 °C / 1 h. After the certain incubation time 5 h the cellular precipitation of M_2N started from grain boundaries (Fig. 3b).

The time-temperature-precipitation (TTP) diagrams were constructed on the base of statistical analysis of the precipitation. The nose temperature of M_2N precipitation was determined to be about 825° C, with corresponding incubation period of precipitation 2.5 min. Fig. 4 shows the relationship between volume fraction of precipitates and annealing time (t) at the different temperatures. The regression curves were constructed based on these data (Fig. 5). According to these curves the diffusion activation energy is determined as about 129 kJ.mol^{-1}. We use Arrhenius equation in logarithmic shape:

$$Q = \frac{R \ln\frac{t_1}{t_2}}{\frac{1}{T_1} - \frac{1}{T_2}} \qquad (1)$$

where t_1 and t_2 is time necessary for selected volume fraction of precipitates and T_1 and T_2 annealing temperature.

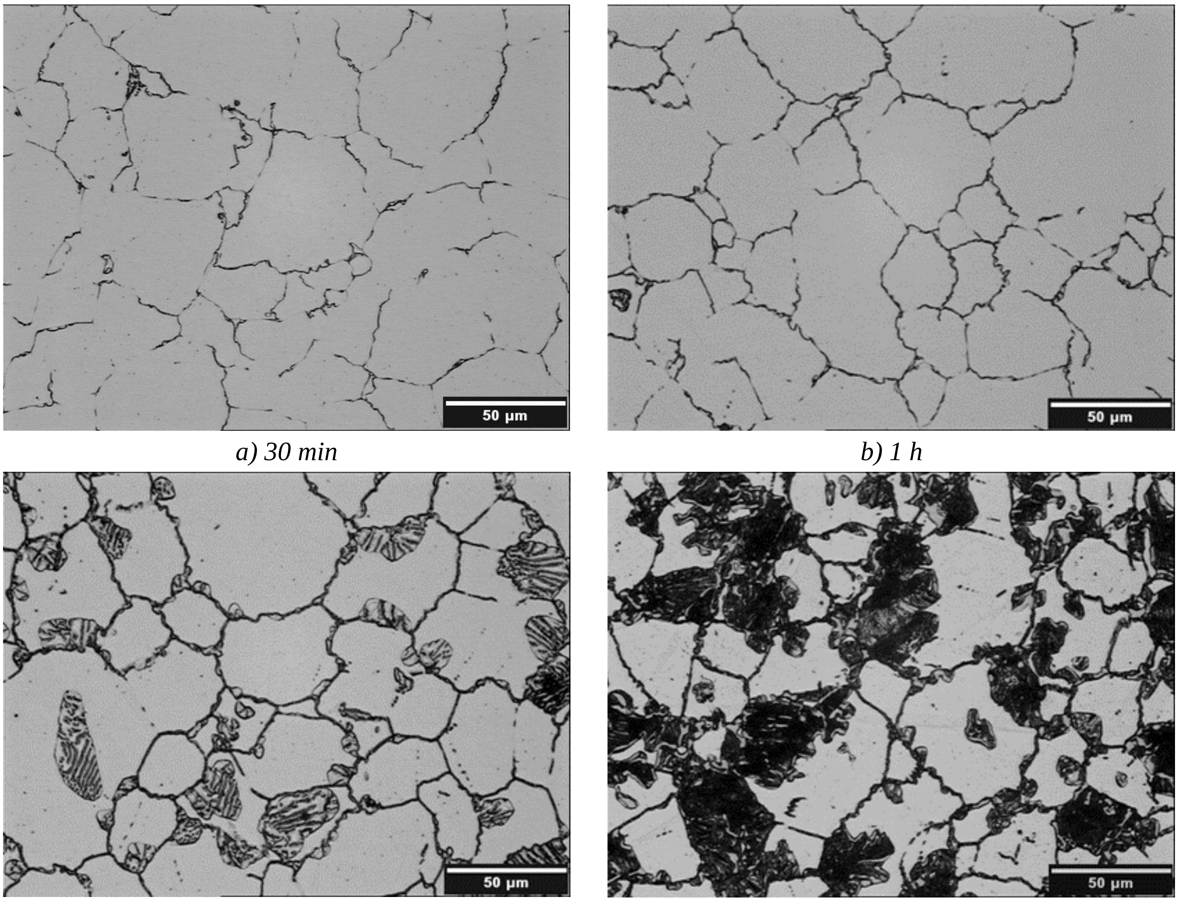

a) 30 min *b) 1 h*

c) 10 h *d) 30 h*

Fig. 1. Microstructure of samples after isothermal annealing at 850° C.

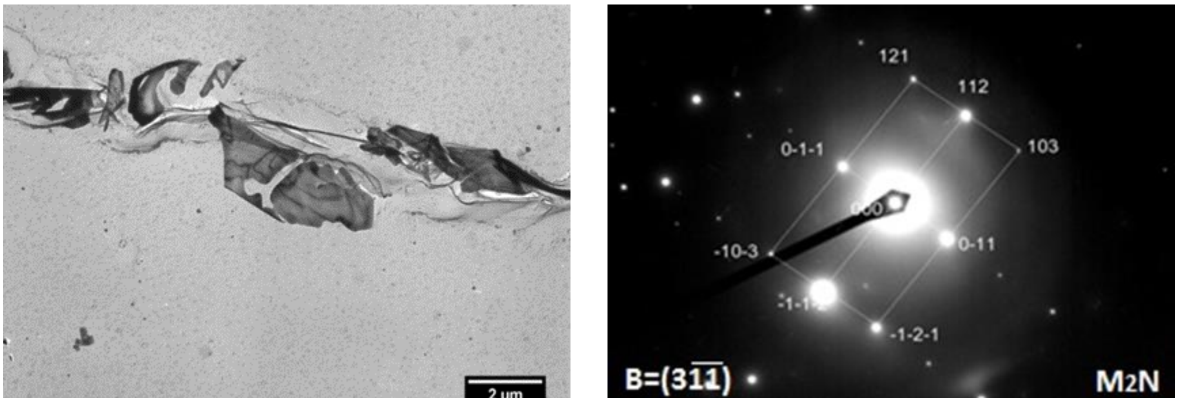

a) detail of grain boundary with the particles of irregular shape 750°C/1 h *b) electron diffraction pattern of particles (SAD)*

Fig. 2. TEM micrograph (replica).

Table 1

Chemical composition of the metal elements of the particles at the grain boundaries in the samples annealed 750 °C / 1 h.

particles	**chemical composition (mass %)**			
	Cr	Fe	Ni	Mo
irregular shape (M_2N)	95.0 ± 2.5	3.5 ± 0.8	1.0 ± 0.5	0.5 ± 0.2

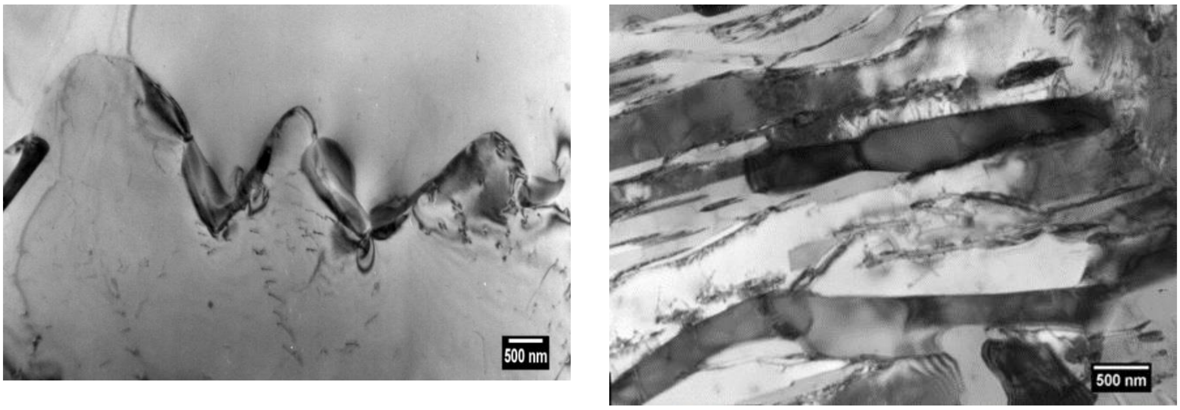

a) detail of the grain boundary serration with the particles of irregular shape (800 °C / 1h)

b) cellular precipitation of nitride M_2N inside grain (800 °C / 5h)

Fig. 3. TEM micrograph (thin foils).

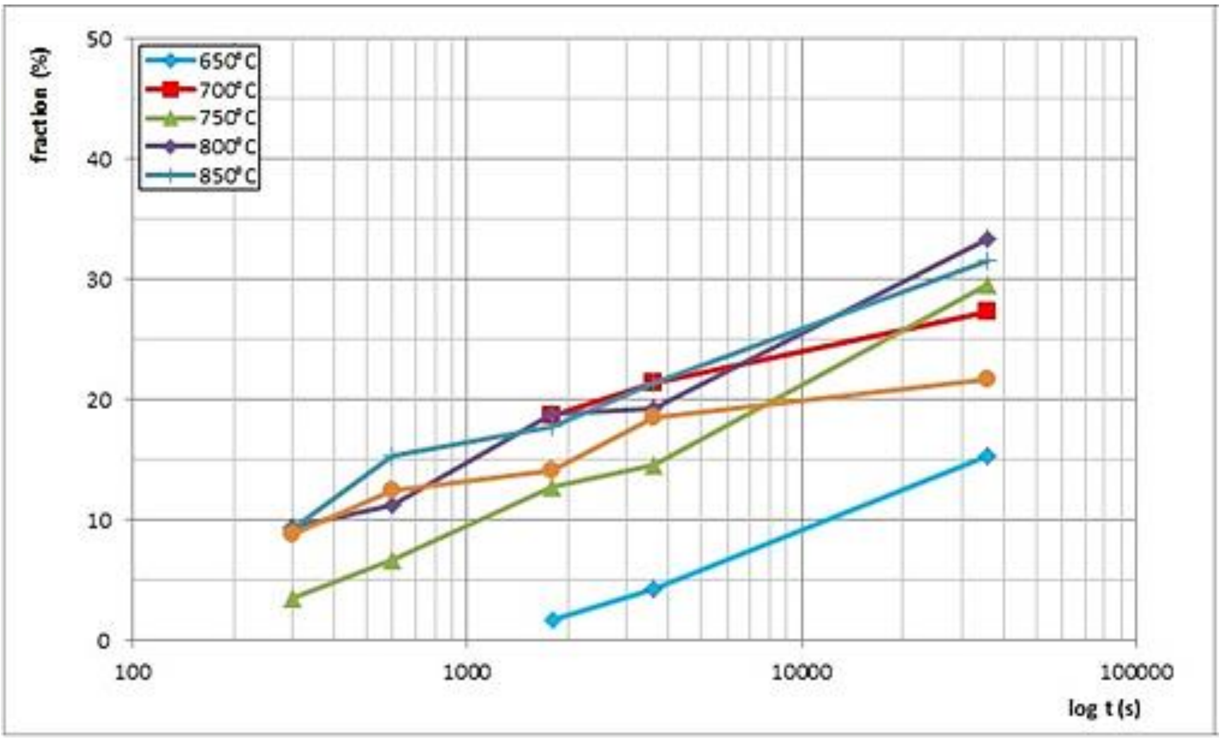

Fig. 4. Relationship between volume fraction of M_2N and annealing time at the different temperatures.
(full colour version available online)

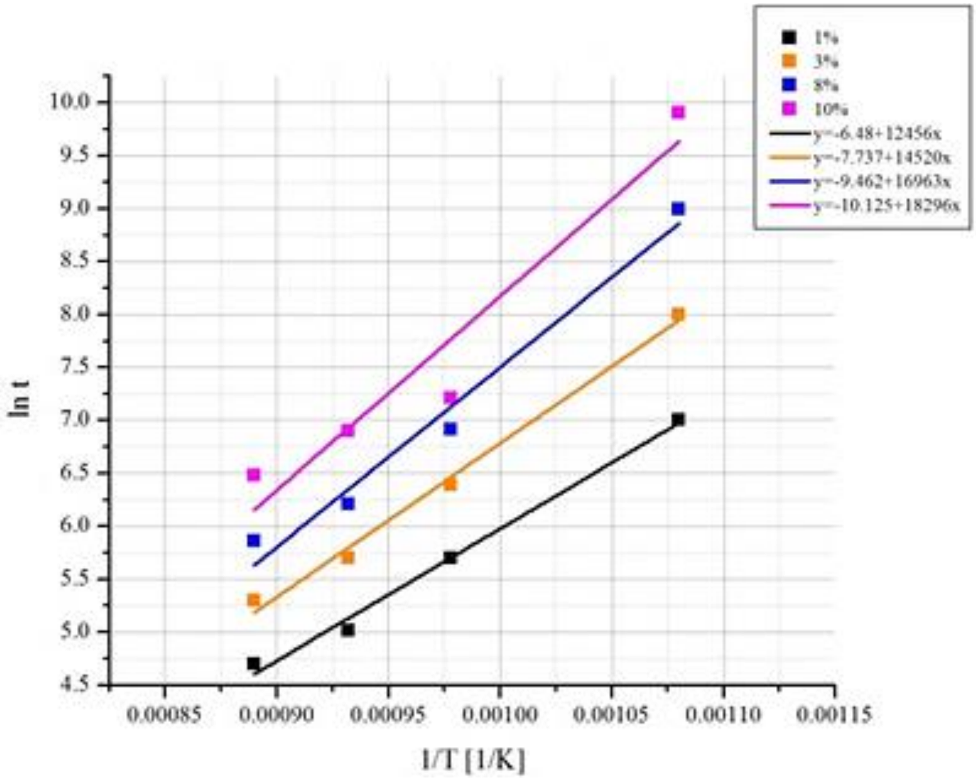

Fig. 5. Regression curves in lower annealing temperatures regions.
(full colour version available online)

4. Conclusions

The precipitation behaviour of CrMnN high nitrogen austenitic stainless steel has been investigated in the temperatures range from 650 to 900°C for duration range from 5 min to 30 h. The following conclusions were drawn:

1. the morphology of M_2N precipitation is transformed from initial irregular shape at the grain boundaries to lamellar ones in the cell as the annealing time increases. The precipitates are first observed to nucleate along grain boundaries in the samples, which were annealed shorter time than 10 hours. As the aging time increases, the precipitates start to grow inward austenitic grains by cellular precipitation, and precipitates in the cell at the early stage of aging are granular. With further increase in the aging time, the cellular precipitation region continues to grow and the granular precipitates in the cell are prolonged,
2. according to the isothermal precipitation kinetics curves of M_2N the nose temperature is about 825 °C with holding time 2.5 min.,
3. diffusion activation energy of M_2N precipitation is about 129 kJ.mol^{-1} for experimental steel.

Acknowledgements

The authors wish to thank the financial support of Scientific Grant Agency of Slovak Republic (VEGA) under grant No. 1/0402/13.

References

[1] L. Kunz, P. Lukáš, R. Konečná, S. Fintová: Int. J. Fatigue 41 (2012) 47-51.

[2] M. Šmíd, V. Horník, P. Hutař, L. Kunz, K. Hrbáček, A. Joch: Slévárenství 9-10 (2015) 340-344 (*in Czech*).

[3] M. Šmíd, K. Obrtlík: Key Eng. Mater. 592–593 (2014) 429–432.

[4] N. Luptáková, N. Pizúrová, P. Roupcová, P. Dymáček: Mater. Eng. – Mater. Inž. 22(2) (2015) 85-94.

[5] J.W. Simmons: Mater. Sci. Eng. A207 (1996) 159-169.

[6] F. Shi, L.J. Wang,W.F. Cui,C.M. Liu: J. Iron Steel Res. Inter. 15(6) (2008) 72-77.

[7] H.B. Li, Z.H. Jiang, H. Feng, Q.F. Ma, D.P. Zhan: J. Iron Steel Res. Inter. 19(8) (2012) 43-51.

[8] P. Skočovský, O. Bokůvka, R. Konečná, E. Tillová: Náuka o materiáli. (*Materials Science*) EDIS UNIZA, Žilina 2006 (*in Slovak*).

[9] Materials Characterization, ASM Metals Handbook Vol. 10, ASM Interational, Ohio 1986.

[10] R.D. Knutsen, C.I.Lang, J.A. Basson: Acta Mater. 52 (2004) 2407-2417

[11] J.C. Rawers: J. Mater. Sci. 43 (2008) 3618-3624